

Vacuum Polarisation and Hadronic Contribution to muon $g - 2$ from Lattice QCD

M. Göckeler^{a,b}, R. Horsley^c, W. Kürzinger^{d,e}, D. Pleiter^d,
P. E. L. Rakow^f, G. Schierholz^{d,g}

^a*Institut für Theoretische Physik, Universität Leipzig,
D-04109 Leipzig, Germany*

^b*Institut für Theoretische Physik, Universität Regensburg,
D-93040 Regensburg, Germany*

^c*School of Physics, University of Edinburgh,
Edinburgh EH9 3JZ, UK*

^d*John von Neumann-Institut für Computing NIC,
Deutsches Elektronen-Synchrotron DESY,
D-15735 Zeuthen, Germany*

^e*Institut für Theoretische Physik, Freie Universität Berlin,
D-14195 Berlin, Germany*

^f*Theoretical Physics Division, Department of Mathematical Sciences,
University of Liverpool, Liverpool L69 3BX, UK*

^g*Deutsches Elektronen-Synchrotron DESY,
D-22603 Hamburg, Germany*

[QCDSF Collaboration]

Abstract

We compute the vacuum polarisation on the lattice in quenched QCD using non-perturbatively improved Wilson fermions. Above Q^2 of about 2 GeV^2 the results are very close to the predictions of perturbative QCD. Below this scale we see signs of non-perturbative effects which we can describe by the use of dispersion relations. We use our results to estimate the light quark contribution to the muon's anomalous magnetic moment. We find the result $446(23) \times 10^{-10}$, where the error only includes statistical uncertainties. Finally we make some comments on the applicability of the Operator Product Expansion to our data.

Key words: QCD, Lattice, e^+e^- Annihilation, muon anomalous magnetic moment
PACS: 11.15.Ha, 12.38.-t, 12.38.Bx, 12.38.Gc, 16.65.+i

1 Introduction

The vacuum polarisation $\Pi(Q^2)$ provides valuable information on the interface between perturbative and non-perturbative physics. It has been the subject of intensive discussions in the literature.

The vacuum polarisation tensor is responsible for the running of α_{em} , which must be known very accurately for high-precision electro-magnetic calculations. To calculate the hadronic contribution to the anomalous magnetic moment of the muon we need to know the vacuum polarisation at scales from ~ 100 MeV to many GeV. Perturbative QCD will be unreliable at the low end of this scale, so a non-perturbative calculation on the lattice would be useful.

The vacuum polarisation $\Pi(Q^2)$ is defined by

$$\Pi_{\mu\nu}(q) = i \int d^4x e^{iqx} \langle 0 | T J_\mu(x) J_\nu(0) | 0 \rangle \equiv (q_\mu q_\nu - q^2 g_{\mu\nu}) \Pi(Q^2), \quad (1)$$

where J_μ is the hadronic electromagnetic current

$$J_\mu(x) = \sum_f e_f \bar{\psi}_f(x) \gamma_\mu \psi_f(x) = \frac{2}{3} \bar{u}(x) \gamma_\mu u(x) - \frac{1}{3} \bar{d}(x) \gamma_\mu d(x) + \dots \quad (2)$$

and $Q^2 \equiv -q^2$ (so that $Q^2 > 0$ for spacelike momenta, $Q^2 < 0$ for timelike). Π can be computed on the lattice for spacelike momenta $Q^2 > 0$.

Π can also be calculated in perturbation theory. Π has to be additively renormalised, even the one-loop diagram (with no gluons involved) is logarithmically divergent. This renormalisation implies that the value of Π can be shifted up and down by a constant depending on scheme and scale without any physical effects. However the Q^2 dependence of $\Pi(Q^2)$ is physically meaningful, and it must be independent of renormalisation scheme or regularisation.

Experimentally Π can be calculated from data for the total cross section of $e^+e^- \rightarrow$ hadrons with theoretical predictions of QCD by means of the dispersion relations [1]

$$12\pi^2 Q^2 \frac{(-1)^n}{n!} \left(\frac{d}{dQ^2} \right)^n \Pi(Q^2) = Q^2 \int_{4m_\pi^2}^{\infty} ds \frac{R(s)}{(s + Q^2)^{n+1}}, \quad (3)$$

where

$$R(s) = \frac{\sigma_{e^+e^- \rightarrow \text{hadrons}}(s)}{\sigma_{e^+e^- \rightarrow \mu^+\mu^-}(s)} = \left(\frac{3s}{4\pi\alpha_{em}^2} \right) \sigma_{e^+e^- \rightarrow \text{hadrons}}(s). \quad (4)$$

The first derivative of the vacuum polarisation (the $n = 1$ term in eq.(3)) is

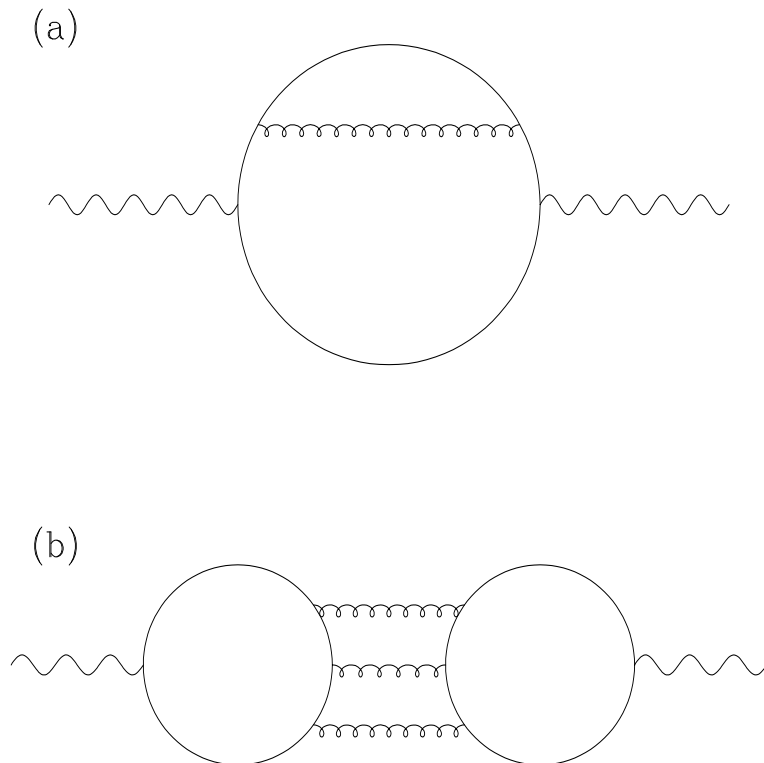


Fig. 1. A typical Feynman diagram contributing to the C_Π part of the vacuum polarisation Π is shown as diagram (a). A diagram contributing to the A_Π part of Π is shown in (b). In this paper we only consider diagrams of the first type, with both photons attached to the same quark line.

referred to as the Adler D -function [2]:

$$D(Q^2) = -12\pi^2 Q^2 d\Pi(Q^2)/dQ^2. \quad (5)$$

The anomalous magnetic moment of the muon $(g - 2)_\mu$ can be calculated to very high order in QED (5 loop), and measured very precisely. $(g - 2)_\mu$ is more sensitive to high-energy physics than $(g - 2)_e$, by a factor m_μ^2/m_e^2 , so it is a more promising place to look for signs of new physics, but to identify new physics we need to know the conventional contributions very accurately. QED perturbative calculations take good account of muon and electron loops, but at the two-loop level quarks can be produced, which in turn will produce gluons. The dominant contribution comes from photons with virtualities $\sim m_\mu^2$, which is a region where QCD perturbation theory will not work well.

$\Pi(Q^2)$ can be split into two contributions with a different dependency on

the quark charges, as shown in Fig.1,

$$-12\pi^2\Pi(Q^2) = \sum_f e_f^2 C_{\Pi}(\mu^2, Q^2, m_f) + \sum_{f,f'} e_f e_{f'} A_{\Pi}(\mu^2, Q^2, m_f, m_{f'}). \quad (6)$$

The C_{Π} term begins with a tree-level term which is $\mathcal{O}(\alpha_s^0)$, while the first contribution to the A_{Π} term is $\mathcal{O}(\alpha_s^3)$. Furthermore, if flavour $SU(3)$ is a good symmetry, the contribution to A_{Π} from the three light flavours (u, d, s) cancels because $e_u + e_d + e_s = 0$, and the only surviving contributions to A_{Π} come when both f and f' are heavy quarks (c, b, t). In this paper we will concentrate on the C_{Π} term, both because it is larger, and because it is much easier to measure on the lattice.

For large (spacelike) momenta $C_{\Pi}(\mu^2, Q^2, m_f)$ can be expressed by means of the Operator Product Expansion, OPE

$$C_{\Pi}(\mu^2, Q^2, m_f) = c_0(\mu^2, Q^2, m_f) + \frac{c_4^F(\mu^2, Q^2)}{(Q^2)^2} m_f \langle \bar{\psi}_f \psi_f \rangle \quad (7)$$

$$+ \frac{c_4^G(\mu^2, Q^2)}{(Q^2)^2} \frac{\alpha_s}{\pi} \langle G_{\mu\nu}^2 \rangle + \frac{c_4'^F(\mu^2, Q^2)}{(Q^2)^2} \sum_{f'} m_{f'} \langle \bar{\psi}_{f'} \psi_{f'} \rangle + \mathcal{O}(1/(Q^2)^3),$$

where c_0 , c_4^F , $c_4'^F$ and c_4^G are the Wilson coefficients and μ is the renormalisation scale parameter in some renormalisation scheme such as \overline{MS} . The f' sum extends over the flavours of the sea quarks (internal quark loops not directly connected to the photon lines). The Wilson coefficients can be computed in perturbation theory, while the non-perturbative physics is encoded in the condensates $m_f \langle \bar{\psi}_f \psi_f(\mu) \rangle$, $\alpha_s \langle G_{\mu\nu}^2(\mu) \rangle$, etc.

Perturbatively the functions D , eq.(5), and R , eq.(4), are known to four loops for massless quarks [3,4], while the coefficient c_0 is known to three loops in the massive case [5]. The coefficients c_4^F , $c_4'^F$ and c_4^G are known up to $\mathcal{O}(\alpha_s^2)$ [6,7,8] for massless quarks.

In this paper we shall compute $\Pi(Q^2)$ on the lattice and compare the result with current phenomenology [9]. Preliminary results of this calculation were presented in [10].

The structure of this paper is as follows. After this Introduction we discuss the lattice setup in Sections 2 and Appendix A. The results are presented in Section 3 and Appendix C. In Section 4 and Appendix B we compare with perturbation theory. In Sections 5 and 6 we present a simple model which describes our lattice data well. In Section 7 we use this model to give a lattice estimate of the hadronic contribution to the muon's anomalous magnetic

moment. Finally in Section 8 we make some comments on the applicability of the Operator Product Expansion, and give our conclusions in Section 9.

2 Lattice Setup

We work with non-perturbatively improved Wilson fermions. For the action and computational details, as well as for results of hadron masses and decay constants, see [11,12,13]. Full details of the vacuum polarisation calculation can be found in [14].

To discretise the hadronic electromagnetic current

$$J_\mu^{em}(x) = \sum_f e_f J_\mu^f(x) \quad (8)$$

we use the conserved vector current

$$J_\mu^f(x) = \frac{1}{2} \left(\bar{\psi}_f(x + a\hat{\mu})(1 + \gamma_\mu)U_\mu^\dagger(x)\psi_f(x) - \bar{\psi}_f(x)(1 - \gamma_\mu)U_\mu(x)\psi_f(x + a\hat{\mu}) \right) \quad (9)$$

where a is the lattice spacing. From now on we work with a Euclidean metric and write

$$J_\mu^f(\hat{q}) = \sum_x e^{iq(x+a\hat{\mu}/2)} J_\mu^f(x) \quad (10)$$

with

$$\hat{q}_\mu = \frac{2}{a} \sin\left(\frac{aq_\mu}{2}\right). \quad (11)$$

On the lattice the photon self-energy Π is not simply given by $\langle J_\mu^f(x)J_\nu^f(0) \rangle$. This is because the lattice Feynman rules include vertices where any number of photons couple to a quark line (not just the single-photon vertex of the continuum) [15]. We are therefore led to define

$$\Pi_{\mu\nu}(\hat{q}) = \Pi_{\mu\nu}^{(1)}(\hat{q}) + \Pi_{\mu\nu}^{(2)}(\hat{q}), \quad (12)$$

with

$$\Pi_{\mu\nu}^{(1)}(\hat{q}) = a^4 \sum_x e^{iq(x+a\hat{\mu}/2-a\hat{\nu}/2)} \langle J_\mu^f(x)J_\nu^f(0) \rangle, \quad (13)$$

and

$$\Pi_{\mu\nu}^{(2)}(\hat{q}) = -a\delta_{\mu\nu} \langle J_\mu^{(2)}(0) \rangle. \quad (14)$$

where

$$J_\mu^{(2)}(x) = \frac{1}{2} \left(\bar{\psi}(x + a\hat{\mu})(1 + \gamma_\mu)U_\mu^\dagger(x)\psi(x) + \bar{\psi}(x)(1 - \gamma_\mu)U_\mu(x)\psi(x + a\hat{\mu}) \right). \quad (15)$$

It then follows that (12) fulfils the Ward identity

$$\hat{q}_\mu \Pi_{\mu\nu}(\hat{q}) = \hat{q}_\nu \Pi_{\mu\nu}(\hat{q}) = 0. \quad (16)$$

The conserved vector current (9) is on-shell as well as off-shell improved [16] in forward matrix elements. In non-forward matrix elements, such as the vacuum polarisation, it needs to be further improved,

$$J_\mu^{\text{imp}}(x) = J_\mu(x) + \frac{1}{2}ia c_{CVC} \partial_\nu \left(\bar{\psi}(x) \sigma_{\mu\nu} \psi(x) \right), \quad (17)$$

where we have some freedom in choosing ∂_ν on the lattice. Any choice must preserve (16), and ideally it should keep $\mathcal{O}(a^2)$ corrections small. Considering the fact that the conserved vector current $J_\mu(x)$ ‘lives’ at $x + a\hat{\mu}/2$, the natural (or naive) choice for the improved operator would be

$$\begin{aligned} J_\mu^{\text{imp}}(\hat{q}) &= J_\mu(\hat{q}) + \frac{1}{2}iac_{CVC} \sum_x e^{iq(x+a\hat{\mu}/2)} \frac{1}{4a} \left(T_{\mu\nu}(x + a\hat{\nu}) \right. \\ &\quad \left. + T_{\mu\nu}(x + a\hat{\mu} + a\hat{\nu}) - T_{\mu\nu}(x - a\hat{\nu}) - T_{\mu\nu}(x + a\hat{\mu} - a\hat{\nu}) \right) \\ &= J_\mu(\hat{q}) + \frac{1}{2}c_{CVC} \cos(aq_\mu/2) \sin(aq_\nu) \sum_x e^{iqx} T_{\mu\nu}(x), \end{aligned} \quad (18)$$

where $T_{\mu\nu}(x) \equiv \bar{\psi}(x) \sigma_{\mu\nu} \psi(x)$. Unfortunately it turns out that this choice introduces very large $\mathcal{O}(a^2Q^2)$ errors into Π . We found that

$$J_\mu^{\text{imp}}(\hat{q}) \equiv J_\mu(\hat{q}) + c_{CVC} \sin(aq_\nu/2) \sum_x e^{iqx} T_{\mu\nu}(x) \quad (19)$$

was a better choice of improved current, because it makes the $\mathcal{O}(a^2Q^2)$ terms much smaller, and so we will adopt this definition. The difference between the definitions (18) and (19) is $\mathcal{O}(a^2Q^2)$, so we are free to choose whichever definition leads to the largest scaling region in Q^2 (both agree at small Q^2).

In Fig.2 we show the unimproved polarisation tensor along with the two different choices of improvement term in the case of free fermions. The best agreement with continuum physics comes from using (19), which is the prescription we will use in the rest of this paper.

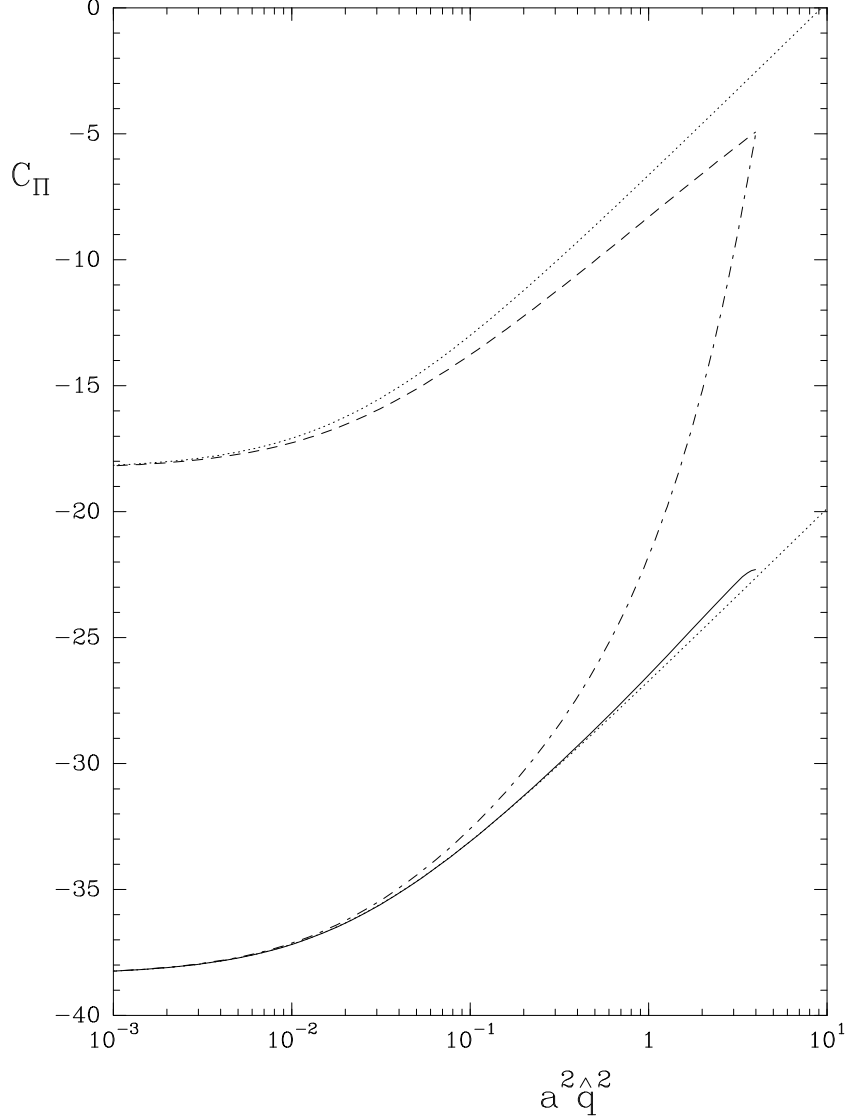


Fig. 2. The effects of improving the current operator. We compare various curves, all calculated in the free-field case at the one-loop level with $q \propto (0, 0, 0, 1)$ and $\kappa = 0.123$ (corresponding to $am = 0.065$). The dotted curves show the continuum one-loop result, shifted vertically to match with lattice results. The dashed line shows the one-loop lattice result without any improvement of the current. The dot-dashed curve shows the result of improving with (18) and the solid curve the result of improving with (19). The upper two curves differ by $O(a)$, the difference $\sim am \ln a^2 \hat{q}^2$. The lower lattice curves are both $O(a)$ improved, but we see that the naive improvement (dot-dashed curve) has very large $O(a^2)$ discretisation errors. Improving with (19) produces a lattice result much closer to the continuum result.

In Appendix A we give explicit expressions for $\Pi_{\mu\nu}^{(1)}(\hat{q})$ and $\Pi_{\mu\nu}^{(2)}(\hat{q})$ in terms of the link variables and the quark propagators.

3 Lattice Calculation

To facilitate the extrapolation to the chiral and continuum limits, we have made simulations at three different values of β with three or more different κ values at each β . The parameters are listed in Table 1. The lattice data for the vacuum polarisation for the individual momenta and β and κ values are given in Appendix C.

β	κ	V	# Conf.
6.0	0.1333	16^4	97
6.0	0.1339	16^4	44
6.0	0.1342	16^4	44
6.0	0.1345	16^4	44
6.0	0.1345	32^4	16
6.2	0.1344	24^4	51
6.2	0.1349	24^4	38
6.2	0.1352	24^4	51
6.4	0.1346	32^4	50
6.4	0.1350	32^4	29
6.4	0.1352	32^4	50

Table 1

Parameters of the lattice simulation. The improvement coefficient in the fermionic action was taken to be $c_{SW} = 1.769$ for $\beta = 6.0$, $c_{SW} = 1.614$ for $\beta = 6.2$ and $c_{SW} = 1.526$ for $\beta = 6.4$ [17].

First, let us discuss the value we use for c_{CVC} . From the fermion-loop contribution to the gluon propagator, computed in [18] to $\mathcal{O}(m)$ in lowest order of lattice perturbation theory, we obtain

$$\begin{aligned}
c_0^{(0)}(\hat{q}^2, am) = & 3 \left(\ln(a^2 \hat{q}^2) - 3am(1 - c_{CVC}) \ln(a^2 \hat{q}^2) - 3.25275141(5) \right. \\
& + 1.19541770(1) c_{CVC} - 7.06903716(4) c_{CVC}^2 \\
& + am \left(6.46270704(30) - 5.29413266(6) c_{CVC} \right. \\
& \left. \left. + 1.67389761(2) c_{CVC}^2 \right) \right) + \mathcal{O}(a^2, m^2),
\end{aligned} \tag{20}$$

where $am = 1/2\kappa - 1/2\kappa_c$. We use $c_0^{(0)}$ to refer to the lowest order, g^0 , per-

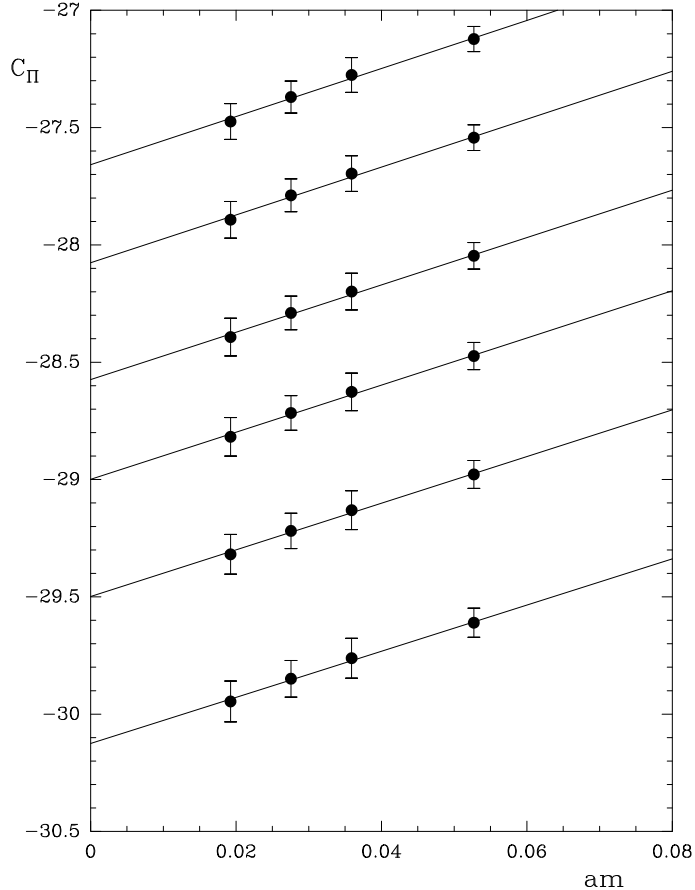


Fig. 3. Chiral extrapolation of $C_{\Pi}(\hat{q}^2, m)$ at $\beta = 6.0$. The points shown range from $a^2\hat{q}^2 \approx 3.0$ to ≈ 6.5 . All are calculated with $c_{CVC} = 1$.

turbative contribution to c_0 . As said earlier, the \hat{q}^2 dependence of Π and c_0 is physical. Therefore in an $O(a)$ -improved calculation there should be no $O(a)$ terms which depend on \hat{q}^2 . On the other hand a constant added to c_0 has no physical effect, so there is no objection to constant terms of $O(a)$ in eq.(20). We see that there is an unphysical $am \ln(a^2\hat{q}^2)$ term in (20) unless $c_{CVC} = 1 + \mathcal{O}(g^2)$. In the following we take $c_{CVC} = 1$ and make the ansatz

$$C_{\Pi}(\hat{q}^2, am) = C_{\Pi}(\hat{q}^2, am = 0) + am M(\hat{q}^2). \quad (21)$$

In Fig. 3 we show the quark mass dependence of $C_{\Pi}(\hat{q}^2, am)$ for several momenta, which justifies assuming a linear am dependence. In Fig. 4 we show the slope $M(\hat{q}^2)$ with and without improvement of the conserved vector current. The derivative M should tend to a constant when $Q^2 \gg m^2$. With no improvement term (open points) we see that M has a logarithmic dependence on \hat{q}^2 , corresponding to an unphysical $am \ln(a^2\hat{q}^2)$ term in c_0 . We see that for $c_{CVC} = 1$ the slope is, within error bars, independent of \hat{q}^2 down to small momenta. This shows that the choice $c_{CVC} = 1$ has eliminated or greatly reduced the unphysical logarithm in c_0 . We conclude that the tree-level value

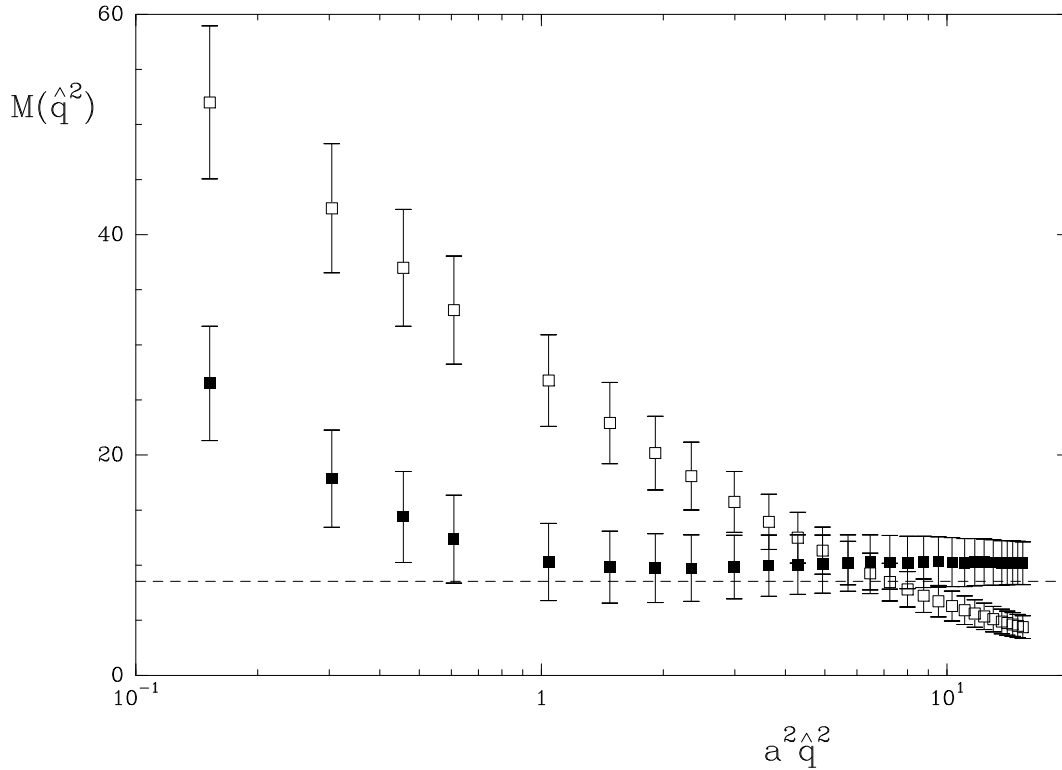


Fig. 4. The slope $M(\hat{q}^2)$ for the improved (solid points, $c_{CVC} = 1$) and unimproved (open points, $c_{CVC} = 0$) vector current as a function of $a^2 \hat{q}^2$ at $\beta = 6.0$. The dashed line shows the height of the plateau in one-loop lattice perturbation theory, setting $c_{CVC} = 1$ in eq.(20).

$c_{CVC} = 1$ is a good choice ¹.

The lattice sizes in Table 1 were chosen such that the physical volume is approximately equal for all three β values. As we have done simulations at $\beta = 6.0$, $\kappa = 0.1345$ on two different lattice volumes we check for finite volume effects. We have not found any, see Fig.5. This figure also shows that on the larger lattice we can measure the vacuum polarisation at much lower values of Q^2 , which is an important advantage. The quark boundary conditions are antiperiodic in all four directions, while gluon and photon fields have periodic boundary conditions in all directions.

¹ If c_{CVC} should ever be computed non-perturbatively, or in perturbation theory, it should be kept in mind that we have used eq. (19) as the definition of the improvement term.

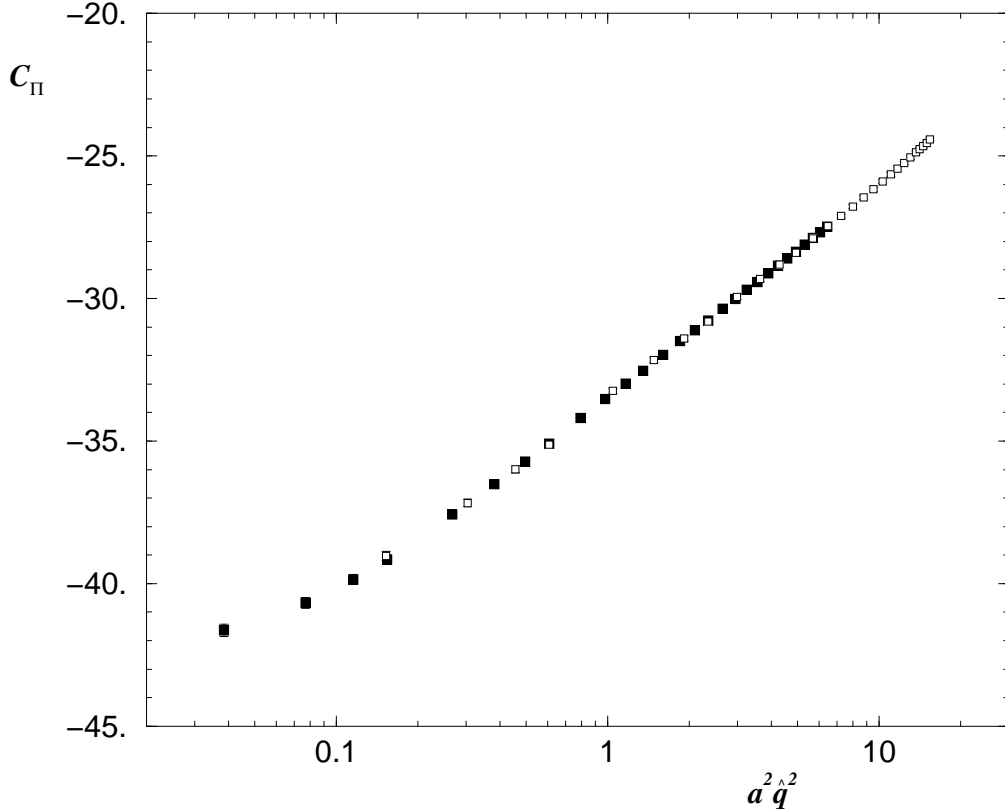


Fig. 5. A check for finite volume effects. At $\beta = 6.0$, $\kappa = 0.1345$ we have measured the polarisation tensor both on a 16^4 lattice (white points) and on a 32^4 lattice (black points). The agreement is excellent, and we conclude that finite volume effects are negligible.

4 Comparison with perturbation theory

The first thing to do is to compare lattice results with continuum perturbation theory, which we do in Fig.6. For the perturbative contribution $c_0^{\text{pert}}(\hat{q}^2, m)$ we use the renormalisation-group improved result given in eqs. (67) and (69) of Appendix B. We use $\Lambda_{\overline{MS}} = 243 \text{ MeV}$ [18,19] and $\mu = 1/a$, and we identify Q^2 with \hat{q}^2 . The r_0 parameter is used to fix the scale [20], with $r_0 = 0.5 \text{ fm}$.

C_{Π} calculated on the lattice and C_{Π} in the continuum can differ by an integration constant which can depend on μ and a . In lowest order perturbation theory this constant is found by comparing $c_0^{(0)}$ in \overline{MS} , eq. (55), with $c_0^{(0)}$ calculated in lattice perturbation theory, eq. (20). Setting c_{CVC} equal to 1 and $\mu = 1/a$ we find that $\Delta c_0 = c_0^{\text{lat}} - c_0^{\overline{MS}} = -22.379$. In next to leading order this becomes

$$\Delta c_0 = -22.379 - 12/11 \ln(\alpha^{\overline{MS}}/\alpha^{\text{lat}}) + \mathcal{O}(\alpha^{\text{lat}}). \quad (22)$$

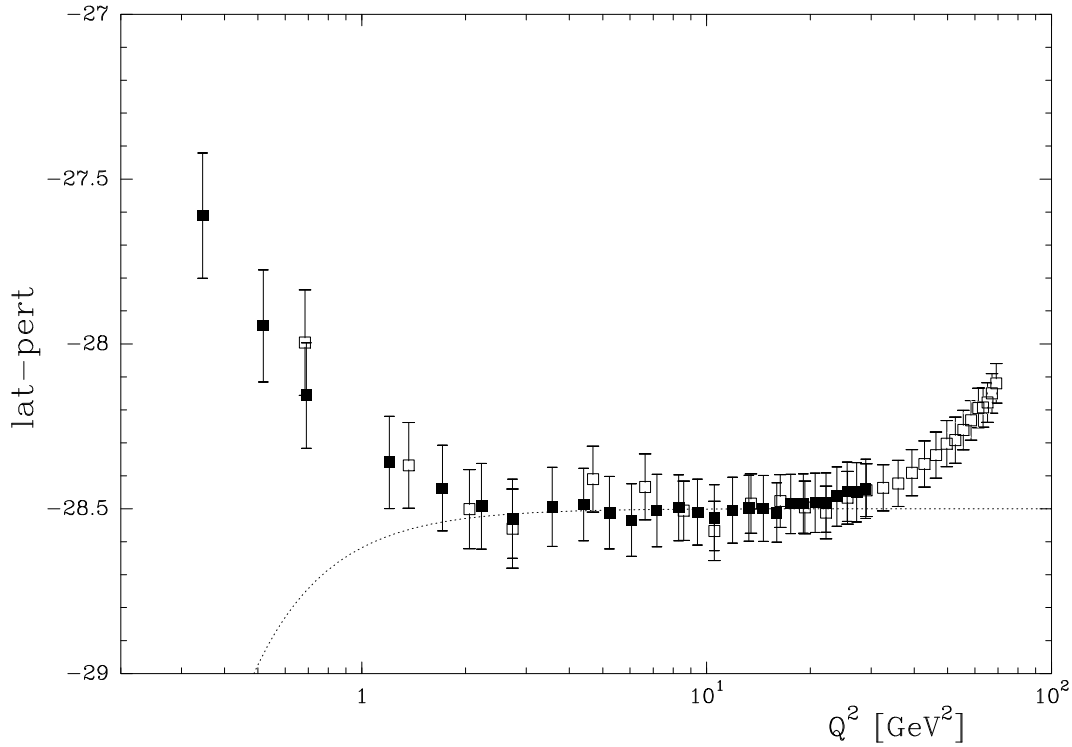


Fig. 6. The deviation of lattice data from continuum perturbation theory. The data are at $\beta = 6.0$, $\kappa = 0.1345$ on a 16^4 lattice (white points) and on a 32^4 lattice (black points). Below $Q^2 \sim 2 \text{ GeV}^2$ there is a visible deviation from perturbation theory. The dotted line shows the effect expected from a gluon condensate as expected in the OPE.

In view of this result, the value $\Delta c_0 \approx -28.5$ seen in Fig.6 is reasonable.

Fig.6 shows that the lattice results deviate from perturbation theory at large Q^2 . This deviation, which sets in at $a^2 \hat{q}^2 \sim 5$, is probably a sign of $O(a^2)$ lattice artefacts.

More interesting are the deviations from perturbation theory at low Q^2 . These are especially large at low quark mass. The OPE, eq.(7), would suggest that the effects of a gluon condensate should show up at small Q^2 . In Fig.6 we show the OPE prediction for a gluon condensate $\frac{\alpha}{\pi} \langle GG \rangle = 0.012 \text{ GeV}^4$. The deviations which we see in the data do not look like the effects expected from a gluon condensate. The sign is the opposite of what the OPE predicts, and the deviation is probably not growing as quickly as $1/Q^4$.

5 A simple model of the vacuum polarisation at low Q^2

We have seen that perturbation theory, even when supplemented with higher twist terms from the operator product expansion, has difficulty in explaining the low Q^2 region of the data. Can we understand this region in some other way?

The cross section ratio $R(s)$ is given by the cut in the vacuum polarisation, or in other words there are dispersion relations which give the vacuum polarisation if we know $R(s)$.

β	κ	am_{PS}	am_V	$1/f_V$
6.0	0.1333	0.4122(9)	0.5503(20)	0.2055(14)
6.0	0.1339	<i>0.3381(15)</i>	<i>0.5017(40)</i>	<i>0.2217(15)</i>
6.0	0.1342	0.3017(13)	0.4904(40)	0.2293(14)
6.0	0.1345	<i>0.2561(15)</i>	<i>0.4701(90)</i>	<i>0.2387(90)</i>
6.2	0.1344	0.3034(6)	0.4015(17)	0.2210(20)
6.2	0.1349	0.2431(6)	0.3663(27)	0.2403(24)
6.2	0.1352	0.2005(9)	0.3431(60)	0.2474(47)
6.4	0.1346	0.2402(8)	0.3107(16)	0.2252(21)
6.4	0.1350	0.1933(7)	0.2800(20)	0.2423(19)
6.4	0.1352	<i>0.1661(10)</i>	<i>0.2613(40)</i>	<i>0.2448(35)</i>

Table 2

Lattice data on the vector meson used as input for the dispersion relation fits [11,13]. Numbers in italics have been interpolated from nearby κ values.

One way of modelling Π is to make a model for $R(s)$, and then calculate Π from R , using the dispersion relation eq.(3). This should be quite robust, since Π gets contributions from a large range in s , little inaccuracies in the model R get washed out, and we can hope that even a crude representation of R will give a good result for Π . We will keep the model simple so that we can do all the integrals analytically.

Perturbatively

$$R(s) = \sum_f e_f^2 N_c \left(1 + \frac{\alpha_s}{\pi} + \dots \right) \quad (23)$$

where N_c is the number of colours (3 in our case). We know that really the low s behaviour of R is more complicated than that, it is dominated by the $\rho(770)$, $\omega(782)$ and $\phi(1020)$ mesons. Following [7], let us make the following model for R . We ignore the splitting between the ρ and ω , which comes from the A_{II} -type diagrams which we have dropped. We also treat these mesons as narrow resonances, each contributing a δ function to R . The continuum part of R takes a while to climb up to the value in eq.(23). We will represent this rise by a step function at some value s_0 . So, our model is

$$R(s) = \sum_f e_f^2 \left(A\delta(s - m_V^2) + B\Theta(s - s_0) \right) \quad (24)$$

where we would expect B to be slightly above 3 in order to match eq.(23).

Using the dispersion relation, this $R(s)$ translates into a vacuum polarisation

$$C_{\text{II}}(Q^2) = B \ln(a^2 Q^2 + a^2 s_0) - A/(Q^2 + m_V^2) + K \quad (25)$$

where K is a constant which is not determined from the dispersion relation, and which never appears in any physical quantity. Again we identify the continuum quantity Q^2 with the lattice quantity \hat{q}^2 .

The constant A can be expressed in terms of the decay constant f_V , which has been measured on the lattice. The cross section for the production of a narrow vector resonance, V , is [7]

$$\sigma_{e^+e^- \rightarrow V}(s) = 12\pi^2 \delta(s - m_V^2) \frac{\Gamma_{V \rightarrow e^+e^-}}{m_V}. \quad (26)$$

The partial width $\Gamma_{V \rightarrow e^+e^-}$ is related to a meson decay constant g_V [21,7] by

$$\Gamma_{V \rightarrow e^+e^-} = \left(\frac{4\pi\alpha_{em}^2}{3} \right) \frac{m_V}{g_V^2}, \quad (27)$$

where

$$\langle 0 | J_\mu^{em} | V, \varepsilon \rangle = \varepsilon_\mu \frac{m_V^2}{g_V}. \quad (28)$$

Here ε_μ is the polarisation vector of the meson. On the lattice it is more natural to define decay constants f_V in terms of currents with definite isospin [11]

$$\langle 0 | \mathcal{V}_\mu | V, \varepsilon \rangle = \varepsilon_\mu \frac{m_V^2}{f_V} \quad (29)$$

with

$$\mathcal{V}_\mu^{I=1} = \frac{1}{\sqrt{2}} (\bar{u}\gamma_\mu u - \bar{d}\gamma_\mu d) \quad (30)$$

for the ρ^0 and

$$\mathcal{V}_\mu^{I=0} = \frac{1}{\sqrt{2}} (\bar{u}\gamma_\mu u + \bar{d}\gamma_\mu d) \quad (31)$$

for the ω (ignoring any $\bar{s}s$ admixture in the ω). The relationship between the two definitions is

$$\frac{1}{g_\rho} = \frac{e_u - e_d}{\sqrt{2}} \frac{1}{f_\rho} = \frac{1}{\sqrt{2}} \frac{1}{f_\rho}, \quad (32)$$

$$\frac{1}{g_\omega} = \frac{e_u + e_d}{\sqrt{2}} \frac{1}{f_\omega} = \frac{1}{3\sqrt{2}} \frac{1}{f_\omega}. \quad (33)$$

In terms of these decay constants

$$R(s) = \sum_V 12\pi^2 \delta(s - m_V^2) \frac{m_V^2}{g_V^2} + \text{continuum} \quad (34)$$

$$\begin{aligned} &= 12\pi^2 \delta(s - m_\rho^2) \frac{m_\rho^2}{f_\rho^2} \frac{(e_u - e_d)^2}{2} \\ &\quad + 12\pi^2 \delta(s - m_\omega^2) \frac{m_\omega^2}{f_\omega^2} \frac{(e_u + e_d)^2}{2} + \text{continuum}. \end{aligned} \quad (35)$$

Neglecting annihilation diagrams implies that $m_\omega = m_\rho$ and $f_\omega = f_\rho$. Experimentally both relations are fairly accurate. The mass ratio m_ω/m_ρ is 1.02. $f_\omega = f_\rho$ implies $\Gamma_{\omega \rightarrow e^+e^-} = \frac{1}{9}\Gamma_{\rho^0 \rightarrow e^+e^-}$, while the experimental ratio is 0.089(5) [22]. Equating the mass and decay constant of the ω and ρ in eq. (35) gives

$$R(s) = 12\pi^2 \delta(s - m_\rho^2) \frac{m_\rho^2}{f_\rho^2} (e_u^2 + e_d^2) + \text{continuum}; \quad (36)$$

so

$$A = 12\pi^2 \frac{m_V^2}{f_V^2}. \quad (37)$$

6 Dispersion relation fits

We first try making fits to the lattice data for the vacuum polarisation C_Π using eq. (25) with B, K and s_0 as free parameters. To avoid problems from lattice artefacts of $\mathcal{O}(a^2 \hat{q}^2)$ we have only used data with $a^2 \hat{q}^2 < 5$. We will call this simple ansatz Fit I. A , the weight of the vector meson contribution, is determined by eq. (37). The vector meson masses and decay constants which we use are shown in Table 2. They have been taken from [11,13]. We can compare the values for B and K with the one-loop lattice perturbation theory result, eq. (20), which gives $B = 3$ and $K = -27.38 + am \ 8.53$.

β	κ	V	$a^2 s_0$	B	K	χ^2
6.0	0.1333	16^4	0.395(32)	3.13(6)	-32.98(11)	4.3
6.0	0.1339	16^4	0.397(43)	3.13(8)	-33.14(14)	2.2
6.0	0.1342	16^4	0.391(39)	3.10(8)	-33.18(13)	3.0
6.0	0.1345	16^4	0.409(61)	3.11(9)	-33.30(16)	2.5
6.0	0.1345	32^4	0.403(79)	3.12(10)	-33.30(18)	0.7
6.2	0.1344	24^4	0.282(21)	3.10(5)	-32.94(7)	1.9
6.2	0.1349	24^4	0.278(24)	3.07(5)	-33.06(8)	1.9
6.2	0.1352	24^4	0.253(25)	3.06(5)	-33.10(7)	2.2
6.4	0.1346	32^4	0.164(13)	3.06(3)	-32.68(5)	0.8
6.4	0.1350	32^4	0.150(14)	3.03(4)	-32.76(6)	0.6
6.4	0.1352	32^4	0.124(12)	3.02(3)	-32.78(5)	1.2

Table 3

The result of Fit I, eq. (25), including only data with $a^2 \hat{q}^2 < 5$.

A typical result is shown in the top panel of Fig.7. As can be seen from Table 3, the χ^2 values for the fits are low in every case. Nevertheless we see that the data deviates quite strongly from the fit when $a^2 \hat{q}^2$ is large. The small deviations from the fit at smaller \hat{q}^2 are not random - they occur in the same place in every data set, and depend on the direction of q . Points where q is near the diagonal direction $(1, 1, 1, 1)$ lie lower than points measured for momenta away from this diagonal direction.

To correct for this behaviour we add terms to our fit to parameterise $\mathcal{O}(a^2)$ lattice errors. There are two possible terms at $\mathcal{O}(a^2)$:

$$a^2 q^2 \quad \text{and} \quad a^2 \frac{\sum_{\mu} q_{\mu}^4}{q^2}. \quad (38)$$

The second term has only cubic symmetry, and can give rise to a dependence of C_{Π} on the direction of q , which would not occur in the continuum. To include these terms we fit with the ansatz (Fit II)

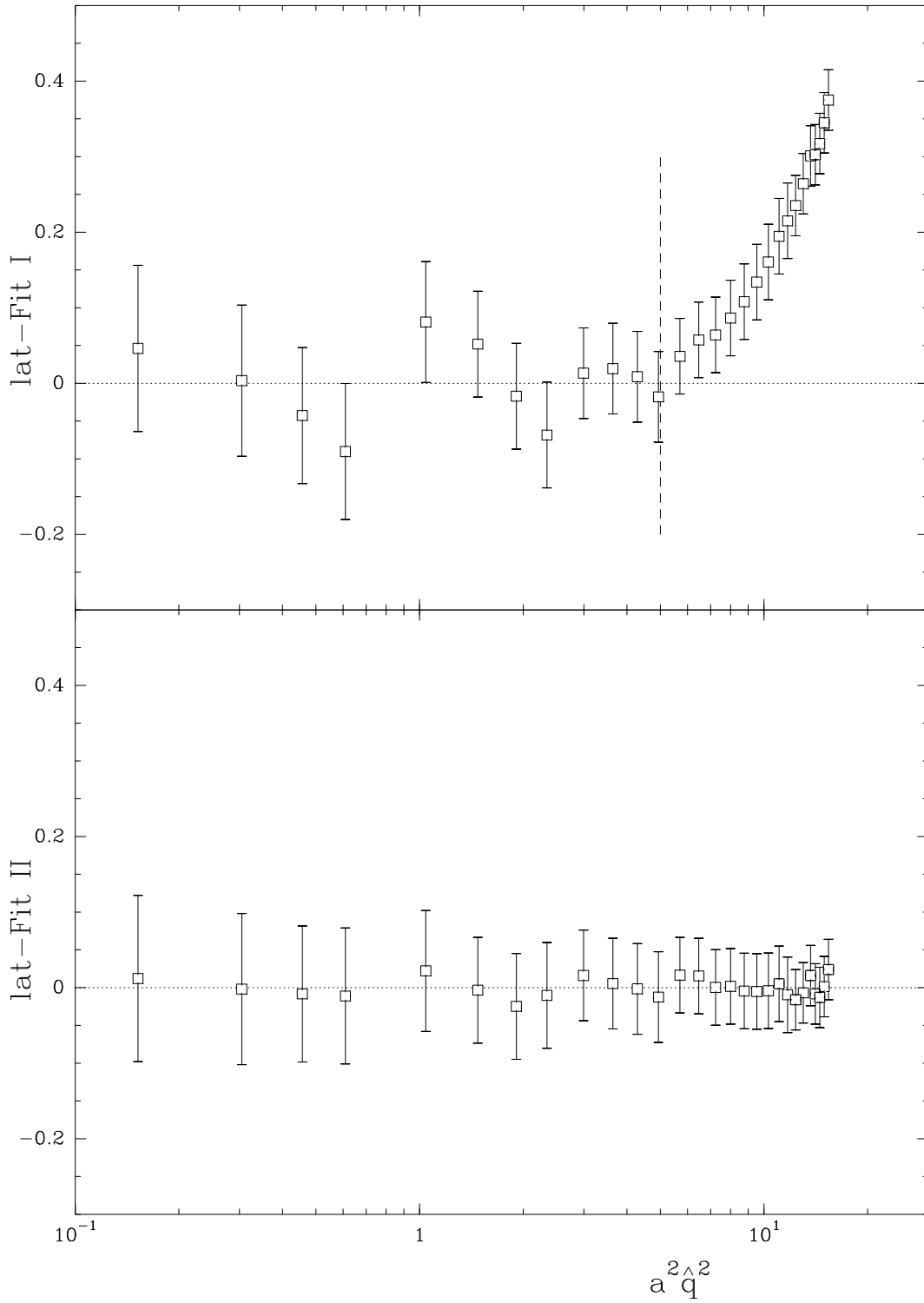


Fig. 7. A comparison between Fit I and Fit II. The data are at $\beta = 6.0$, $\kappa = 0.1333$ on a 16^4 lattice. Fit I only uses data with $a^2 \hat{q}^2 < 5$ (vertical dashed line). The second fit describes the data better.

$$C_{\Pi}(\hat{q}^2) = B \ln(a^2 \hat{q}^2 + a^2 s_0) - \frac{A}{\hat{q}^2 + m_V^2} + K + U_1 a^2 \hat{q}^2 + U_2 h(q) \quad (39)$$

where

$$h(q) = \frac{\sum_{\mu} \sin^4 a q_{\mu} - \frac{1}{4} \left(\sum_{\mu} \sin^2 a q_{\mu} \right)^2}{a^2 \hat{q}^2} \approx a^2 \left[\frac{\sum_{\mu} q_{\mu}^4}{q^2} - \frac{1}{4} q^2 \right]. \quad (40)$$

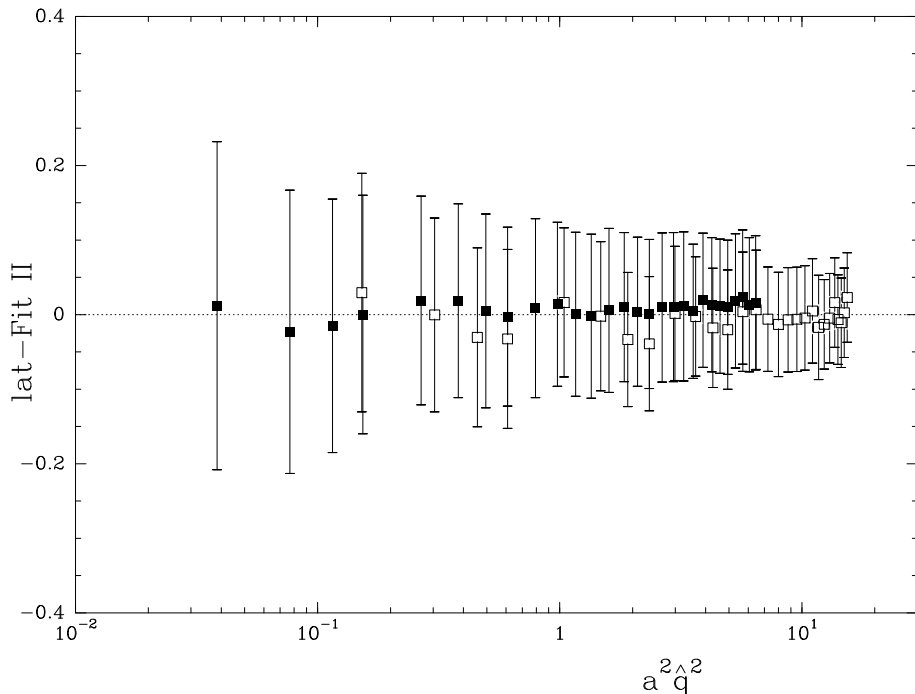


Fig. 8. The deviation of lattice data from the fit of Table 4. The data are at $\beta = 6.0$, $\kappa = 0.1345$ on a 16^4 lattice (white points) and on a 32^4 lattice (black points). The fit describes the data extremely well.

The function $h(q)$ has been chosen so that it vanishes when $q \propto (1, 1, 1, 1)$, as most of our momenta are near this direction. Looking at the lower panel of Fig. 7 we see that the U_1 term does a good job of describing the high \hat{q}^2 data, while the U_2 term successfully describes the direction dependence of the data. Fits with the ansatz (39) show practically no deviation from the data. This can also be seen in Fig.8, where we show the deviation in the case where we have data on two lattice sizes.

In Fig.9 we show the results converted into physical units. The agreement between the different β values is fair, and the value of s_0 in agreement with phenomenology (for example, [23] finds $s_0 = 1.66(22)$ GeV² in the I=1 channel).

In Fig.10 we show the values for the fit parameter B . The value we find is always very close to the tree-level value 3.

β	κ	V	$a^2 s_0$	B	K	χ^2
6.0	0.1333	16^4	0.357(50)	3.00(12)	-32.97(17)	1.52
6.0	0.1339	16^4	0.357(68)	2.99(16)	-33.13(23)	0.69
6.0	0.1342	16^4	0.354(62)	2.97(15)	-33.18(21)	0.83
6.0	0.1345	16^4	0.37(10)	2.97(17)	-33.30(25)	0.70
6.0	0.1345	32^4	0.35(11)	2.92(33)	-33.22(28)	0.06
6.0	0.1345	$16^4 \& 32^4$	0.358(77)	2.93(11)	-33.22(15)	1.49
6.2	0.1344	24^4	0.262(35)	3.00(12)	-32.94(12)	0.14
6.2	0.1349	24^4	0.252(40)	2.94(13)	-33.05(14)	0.12
6.2	0.1352	24^4	0.232(38)	2.95(12)	-33.11(12)	0.13
6.4	0.1346	32^4	0.156(21)	3.01(11)	-32.69(7)	0.08
6.4	0.1350	32^4	0.144(23)	2.99(12)	-32.78(9)	0.10
6.4	0.1352	32^4	0.117(18)	2.97(10)	-32.81(7)	0.11

Table 4

The result of Fit II, including all data.

7 The anomalous magnetic moment of the muon

With a good description of the vacuum polarisation tensor in the low Q^2 region we can make statements about phenomenologically interesting quantities such as the contribution of the u , d and s -quarks to the muon anomalous magnetic moment [24].

Traditionally the hadronic contribution to the muon's anomalous magnetic moment is found from $R(s)$ via a dispersion relation (see [25] for a review)

$$a_\mu^{had} = \frac{\alpha_{em}^2}{3\pi^2} \int_{4m_\pi^2}^{\infty} \frac{ds}{s} K\left(\frac{s}{m_\mu^2}\right) R(s) \quad (41)$$

where

$$K\left(\frac{s}{m_\mu^2}\right) = \int_0^1 \frac{x^2(1-x)}{x^2 + (1-x)s/m_\mu^2} dx. \quad (42)$$

The muon mass, m_μ , is 105.7 MeV. For us it is more useful to deform the contour and find this same number from the vacuum polarisation at spacelike momenta [24]

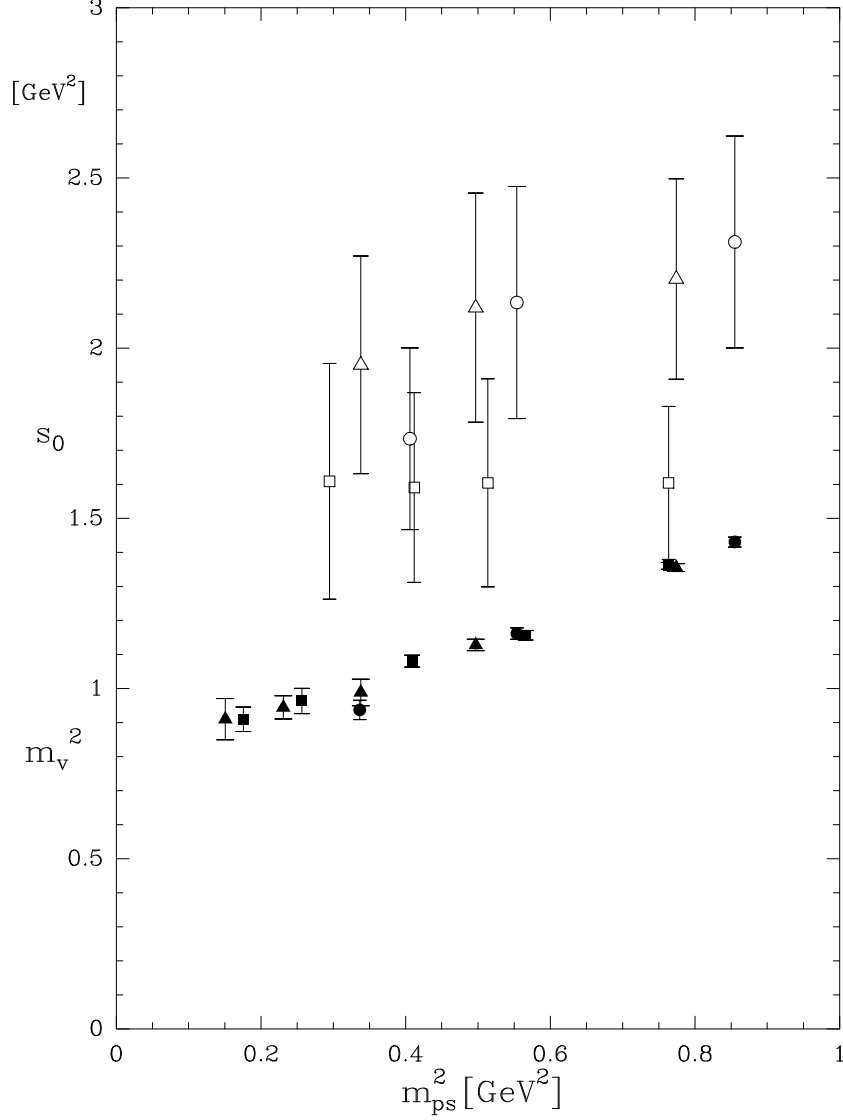


Fig. 9. The threshold s_0 (white points) compared with m_ρ^2 (black points). Squares are for $\beta = 6.0$, triangles for 6.2, and circles for 6.4.

$$\begin{aligned}
a_\mu^{had} &= \frac{\alpha_{em}^2}{3\pi^2} \int_0^\infty \frac{dQ^2}{Q^2} F\left(\frac{Q^2}{m_\mu^2}\right) 12\pi^2 [\Pi(0) - \Pi(Q^2)] \\
&= \frac{\alpha_{em}^2}{3\pi^2} \sum_f e_f^2 \int_0^\infty \frac{dQ^2}{Q^2} F\left(\frac{Q^2}{m_\mu^2}\right) [C_\Pi(Q^2, m_f) - C_\Pi(0, m_f)] \\
&\quad + \text{annihilation} ,
\end{aligned} \tag{43}$$

where the kernel F is

$$F\left(\frac{Q^2}{m_\mu^2}\right) = \frac{16 m_\mu^4}{(Q^2)^2 (1 + \sqrt{1 + 4m_\mu^2/Q^2})^4 \sqrt{1 + 4m_\mu^2/Q^2}} . \tag{44}$$

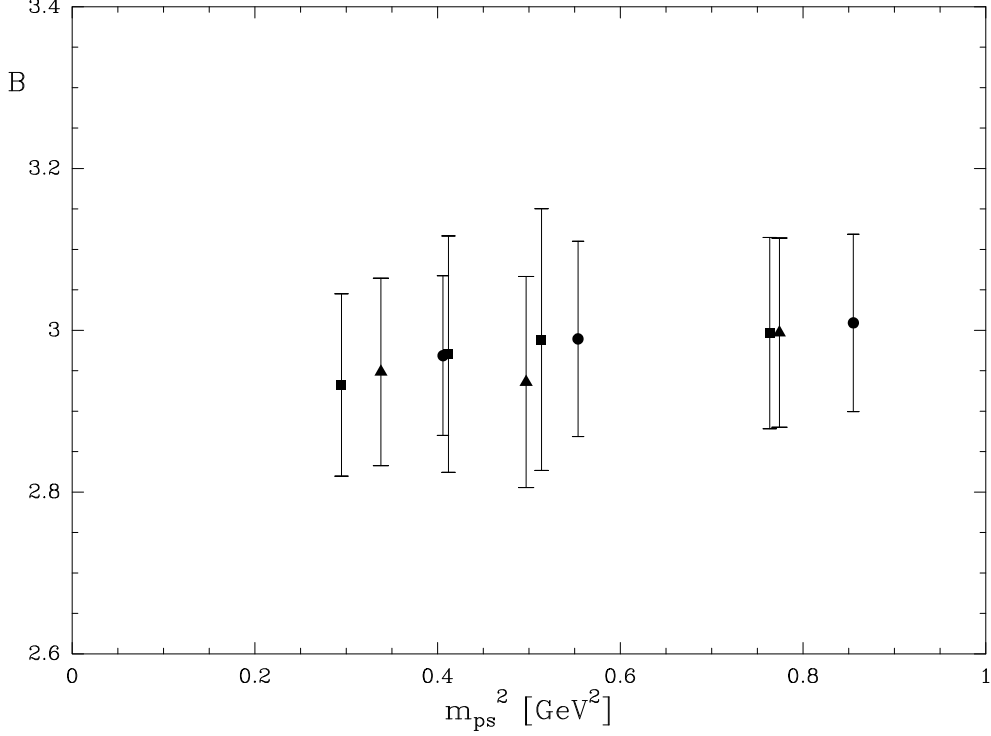


Fig. 10. The parameter B from Table 4. The β values are shown by the same symbols as in Fig.9.

To calculate the value a_μ^{had} we evaluate the integral

$$I^f(m_f) = \int_0^\infty \frac{dQ^2}{Q^2} F\left(\frac{Q^2}{m_\mu^2}\right) [C_\Pi(Q^2, m_f) - C_\Pi(0, m_f)] \quad (45)$$

for each of our data sets. We then need to extrapolate (or interpolate) to the chiral limit (for the u and d quarks) and to the strange quark mass. As can be seen in Fig.11 the integral is dominated by $Q^2 \sim 3m_\mu^2$, so we need to extrapolate in Q^2 , as our lowest measured value is at $Q^2 = 0.17 \text{ GeV}^2$. We do our extrapolation of C_Π by using the results of Fit II from the previous section.

The results are shown in Fig.12, plotted against m_{PS}^2 (the square of the pseudoscalar mass). We see that I depends strongly on the quark mass, with heavier quarks making a smaller contribution (as one would expect). There is also some dependence on β . To extrapolate to the continuum we fit the data with an ansatz of the form

$$I^f = (A_1 + A_2 a^2) + (B_1 + B_2 a^2) m_\pi^2 \quad (46)$$

This describes the data well ($\chi^2/\text{dof} = .53$), and gives the continuum limit shown by the dashed line in Fig.12. The physically relevant values of I^f are at the physical pion mass ($M^2 = 0.019 \text{ GeV}^2$) for the u and d quarks, and at

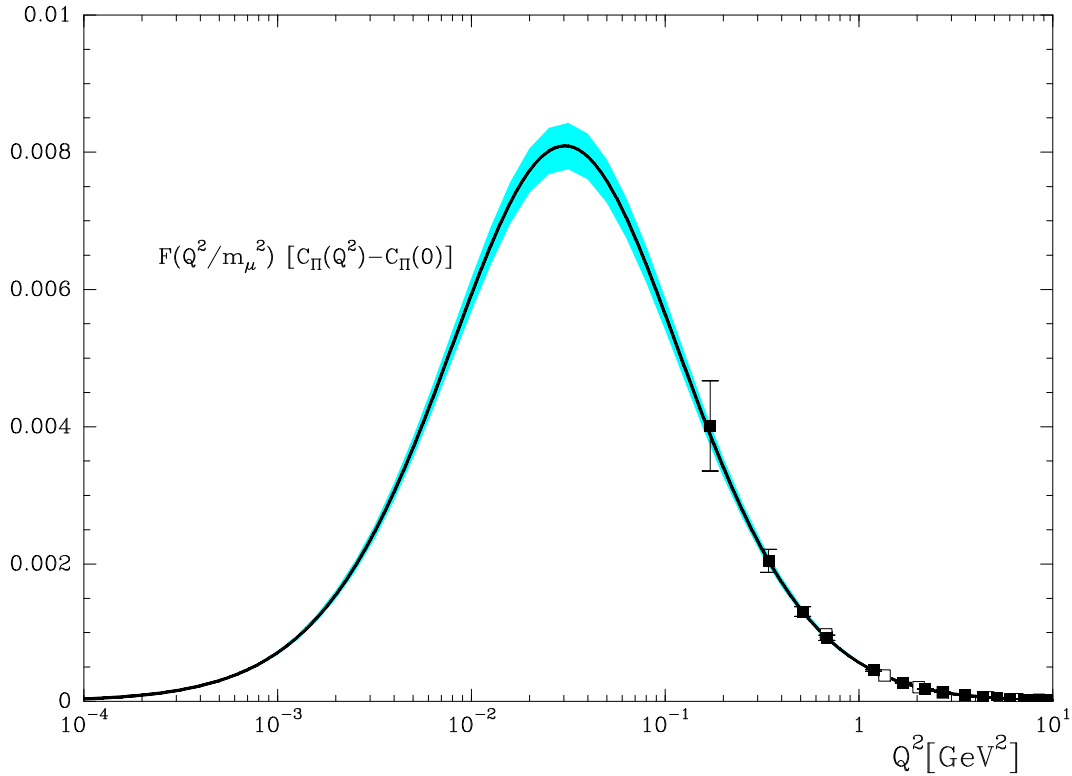


Fig. 11. The product $F(Q^2/m_\mu^2) [C_\Pi(Q^2, m_f) - C_\Pi(0, m_f)]$ for the case $\beta = 6.0$, $\kappa = 0.1345$. The shaded region shows the uncertainty.

the mass of a hypothetical $\bar{s}s$ pseudoscalar meson with $M^2 = 2m_K^2 - m_\pi^2 = 0.468 \text{ GeV}^2$ for I^s . The values at these points are

$$I^u = I^d = 0.0389(21), \quad I^s = 0.0287(9). \quad (47)$$

This gives as our final lattice estimate of a_μ^{had}

$$a_\mu^{had} = \frac{\alpha_{em}^2}{3\pi^2} \left(\frac{4}{9}I^u + \frac{1}{9}I^d + \frac{1}{9}I^s \right) = 446(23) \times 10^{-10}. \quad (48)$$

This error reflects the statistical errors of the lattice calculation and the extrapolations to the physical points. It does not include any estimate of the error due to the quenched approximation used in the calculation. This value is somewhat lower than the experimental value $692.4 \pm 5.9_{exp} \pm 2.4_{radiative} \times 10^{-10}$, found by applying eq. (41) to experimental R measurements [26,27]. Our value is similar to another lattice measurement [24], which finds $460(78) \times 10^{-10}$.

The shortfall in the value of a_μ^{had} can probably be attributed to quenching. In particular a quenched calculation omits the process $e^+e^- \rightarrow \pi\pi$, which is the only contribution allowed at very low s .

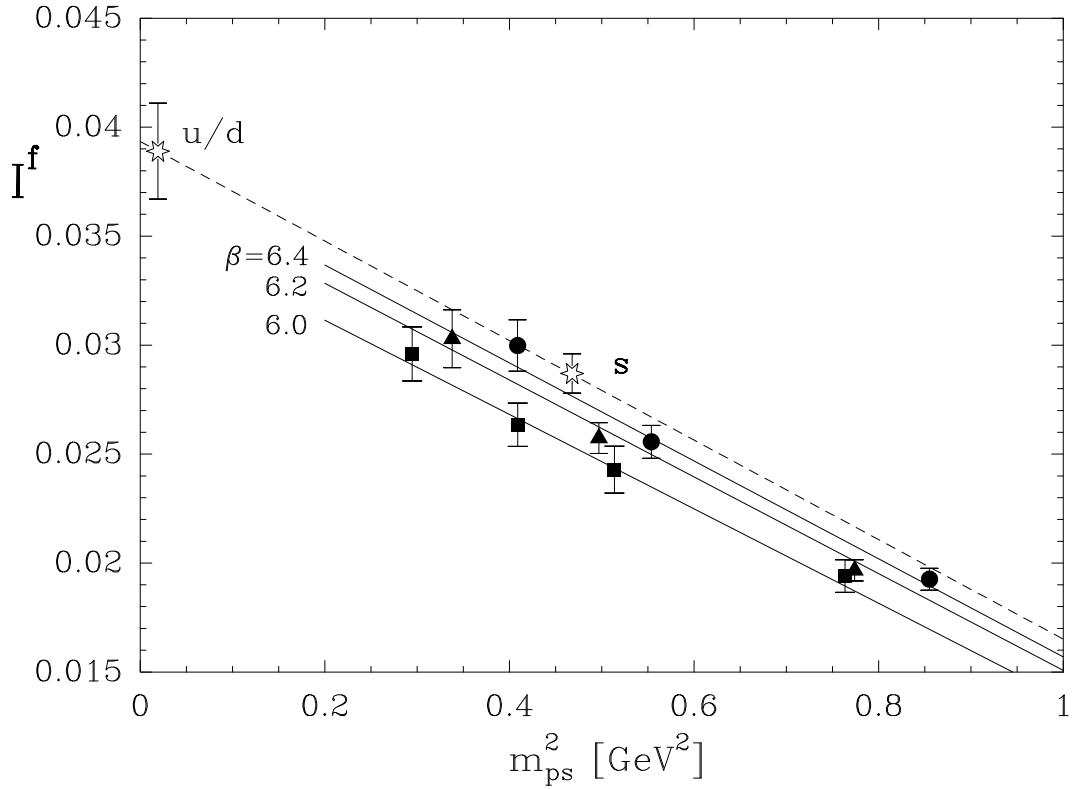


Fig. 12. The results of the integral (45). The β values are shown by the same symbols as in Fig.9. The dashed line shows our extrapolation to the continuum limit, and the points shown with stars are our results for the light (u, d) and strange quarks.

8 The applicability of the Operator Product Expansion

What does the success of our fit function eq. (24) tell us about the applicability and usefulness of the OPE?

To answer this question let us look at the large Q^2 behaviour of the formula (25):

$$\begin{aligned}
C_{\Pi}(Q^2) &= B \ln(Q^2) + K + \frac{Bs_0 - A}{Q^2} + \frac{Am_\rho^2 - \frac{B}{2}s_0^2}{(Q^2)^2} + \dots \\
&= B \ln(Q^2) + K + \sum_{n=1}^{\infty} (-1)^n \left\{ A(m_\rho^2)^{n-1} - \frac{B}{n}s_0^n \right\} (Q^2)^{-n}. \quad (49)
\end{aligned}$$

The expansion has the same form as the OPE, at least at leading order when there are no logarithmic corrections to the Wilson coefficients. We can now look at the higher twist terms in the expansion, and estimate how important

they are in comparison with the gluon condensate contribution.

By looking at the first few terms we can relate our parameters s_0 and A to the condensates in the OPE. In the chiral limit there is no $1/Q^2$ term, so

$$A = Bs_0. \quad (50)$$

This says that the area under the meson δ -function is the same as the grey area in Fig.13, a typical sum-rule style result. Substituting this into the $1/Q^4$ term we get

$$Bs_0 \left(m_\rho^2 - \frac{1}{2}s_0 \right) = -\pi^2 \frac{\alpha_s}{\pi} \langle GG \rangle. \quad (51)$$

Again, a typical sum-rule result — if there were no gluon condensate, the meson would lie at $\frac{1}{2}s_0$, exactly in the middle of the gap. Putting $m_\rho^2 = 0.6 \text{ GeV}^2$ (the physical value) and $\frac{\alpha_s}{\pi} \langle GG \rangle = 0.012 \text{ GeV}^4$ gives $s_0 = 1.26 \text{ GeV}^2$.

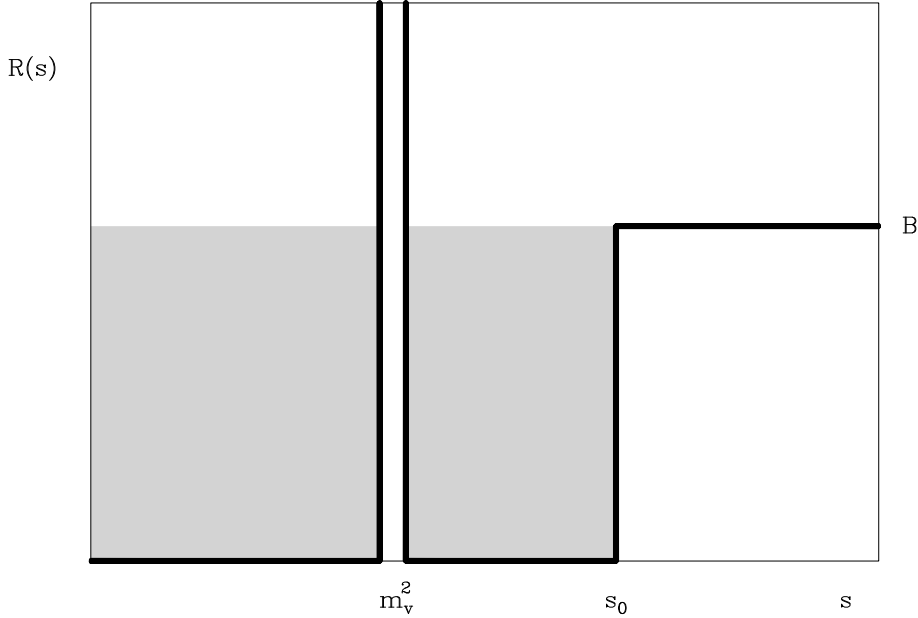


Fig. 13. Our simple model for the contribution of the u and d quarks to $R(s)$.

Next, in Fig.14, we plot a comparison of the threshold model, eq.(25), perturbation theory (just $3 \ln a^2 Q^2$ at this level) and perturbation theory plus the gluon condensate contribution, which scales like $1/(Q^2)^2$. The physically irrelevant constant K has been set to 0 in all cases.

The curve from the threshold model looks physically sensible, it goes to a finite value at $Q^2 = 0$, which is what must happen if $R(s)$ doesn't extend all the way down to $s = 0$.

However, even though we chose our parameters A and s_0 so that the threshold model would match the gluon condensate prediction at high Q^2 , the two

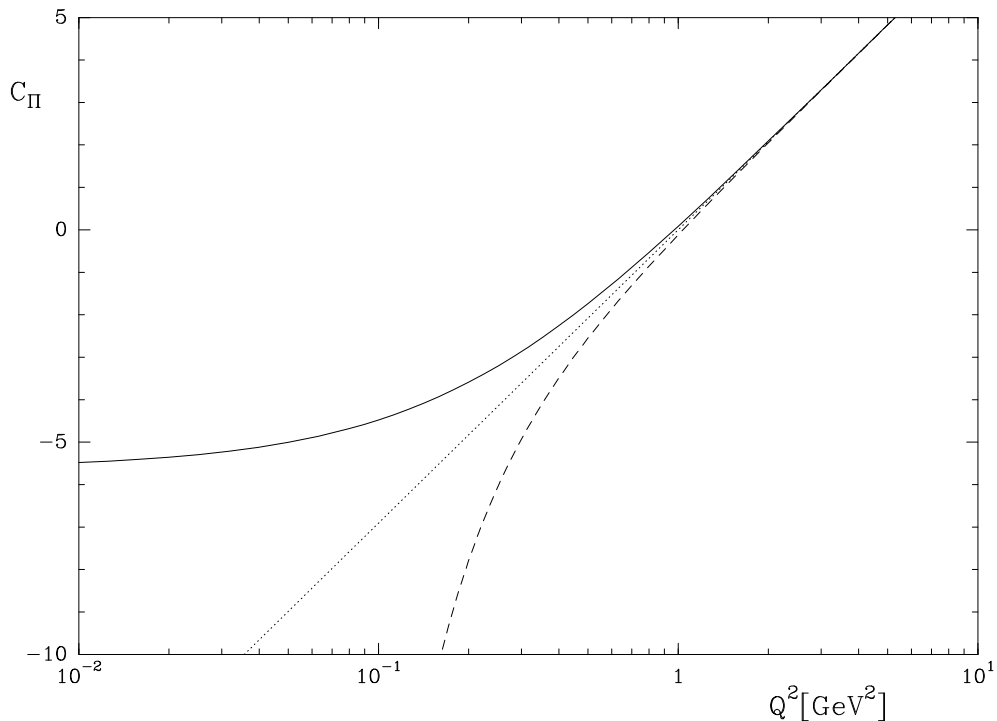


Fig. 14. A comparison of the threshold model, eq.(25) (solid line), perturbation theory (dotted line) and perturbation theory plus the gluon condensate contribution (dashed line). In this plot we have chosen the physically irrelevant constant K to be 0 when all quantities are expressed in GeV.

curves don't resemble each other closely.

Let us now subtract out the perturbative piece, to see things more clearly, Fig.15. We can only find a region where the gluon condensate region is important when we concentrate on the large Q^2 region. If Fig.15 is what the real world looks like, the prospects for getting at the gluon condensate look poor. The gluon condensate term is overwhelmed by higher order terms in the OPE before it has a chance to get significant.

What is the conclusion of this exercise? In the region where we can easily see deviations from perturbation theory the OPE is not very useful, because many operators of very high dimension are all contributing, not just the leading $1/(Q^2)^2$ contribution coming from the gluon condensate. To see the gluon condensate uncontaminated by higher order operators we would need to look in the region $Q^2 \sim 10 \text{ GeV}^2$ with very accurate data (error bars at least 2 orders of magnitude smaller than in this paper). This is unfortunately not a realistic prospect.

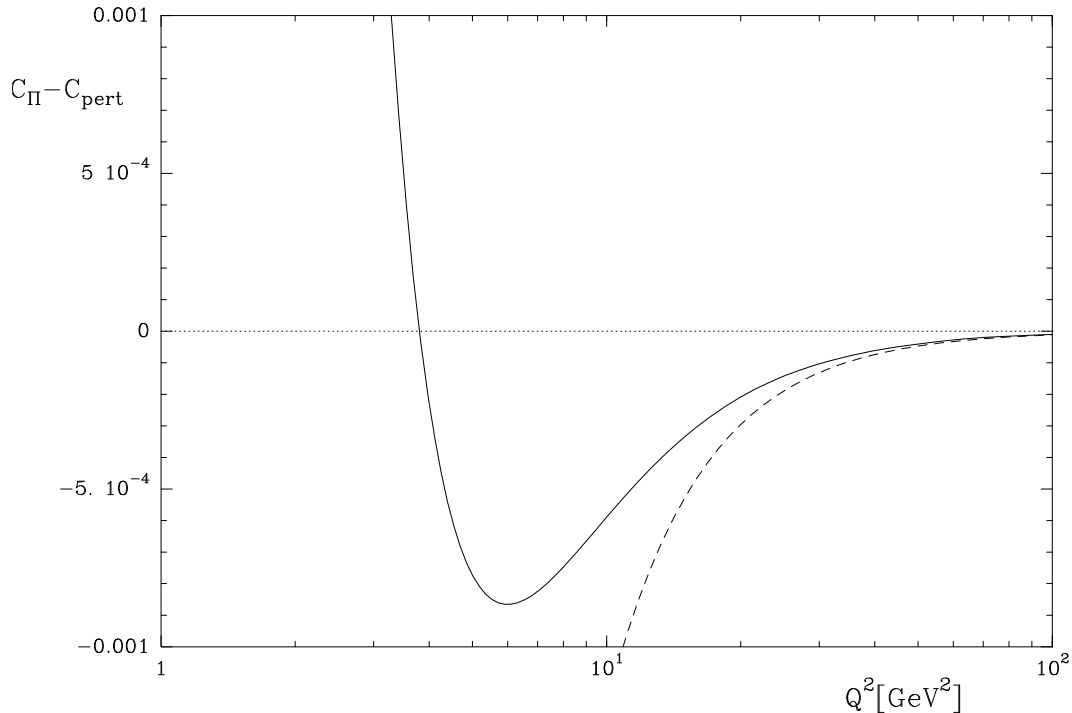


Fig. 15. The same as Fig.14, but with the perturbative piece subtracted. Note that in this figure we are concentrating on the behaviour at rather large Q^2 where non-perturbative effects are small.

9 Conclusions

We have computed the vacuum polarisation in the limit of two light flavours in quenched QCD for three β values (6.0, 6.2 and 6.4) and on lattices as large as 32^4 . It was important to improve the action and the vector current. We found good agreement with three-loop perturbation theory in the interval $2 \lesssim Q^2 \lesssim 20 \text{ GeV}^2$. The lattice data show some indication of non-perturbative effects at the lower end of the Q^2 range. We can describe these very well with a model of $R(s)$ which includes vector mesons and threshold effects. In order to make firm predictions, we need more data at small Q^2 and at smaller lattice spacings with high statistics.

From the low Q^2 region of the vacuum polarisation we can extract a lattice value for a_μ^{had} , the hadronic contribution to the muon's anomalous magnetic moment. We find the value $446(23) \times 10^{-10}$ which is of the right order of magnitude, though lower than the physical value. Our estimate could be improved by using a larger lattice size, enabling us to reach lower Q^2 which would reduce uncertainties from extrapolation. Naturally, dynamical calculations would be very interesting.

Acknowledgements

The numerical calculations were performed on the Quadrics computers at DESY Zeuthen. We thank the operating staff for their support. This work was supported in part by the European Community's Human Potential Program under Contract HPRN-CT-2000-00145, Hadrons/Lattice QCD, as well as by the DFG (Forschergruppe Gitter-Hadronen-Phänomenologie) and BMBF.

We would like to thank C. Michael and T. Teubner for useful comments.

Appendix A

We denote the quark propagator from lattice points x to y by $G(x, y)$. For $\Pi_{\mu\nu}^{(1)}(\hat{q})$ we then obtain

$$\begin{aligned}
\Pi_{\mu\nu}^{(1)}(\hat{q}) &= \frac{a^4}{4} \sum_x e^{iq(x+a\hat{\mu}/2-a\hat{\nu}/2)} \\
&\quad \text{Tr} \left\langle (1 + \gamma_\nu) U_\nu^\dagger(0) \gamma_5 G^\dagger(x + a\hat{\mu}, 0) \gamma_5 (1 + \gamma_\mu) U_\mu^\dagger(x) G(x, a\hat{\nu}) \right. \\
&\quad - (1 - \gamma_\nu) U_\nu(0) \gamma_5 G^\dagger(x + a\hat{\mu}, a\hat{\nu}) \gamma_5 (1 + \gamma_\mu) U_\mu^\dagger(x) G(x, 0) \\
&\quad - (1 + \gamma_\nu) U_\nu^\dagger(0) \gamma_5 G^\dagger(x, 0) \gamma_5 (1 - \gamma_\mu) U_\mu(x) G(x + a\hat{\mu}, a\hat{\nu}) \\
&\quad \left. + (1 - \gamma_\nu) U_\nu(0) \gamma_5 G^\dagger(x, a\hat{\nu}) \gamma_5 (1 - \gamma_\mu) U_\mu(x) G(x + a\hat{\mu}, 0) \right\rangle \\
&- \frac{a^5}{4} c_{CVC} \sum_x e^{iq(x+a\hat{\mu}/2)} \hat{q}_\lambda \\
&\quad \text{Tr} \left\langle (1 + \gamma_\mu) U_\mu^\dagger(x) G(x, 0) \sigma_{\nu\lambda} \gamma_5 G^\dagger(x + a\hat{\mu}, 0) \gamma_5 \right. \\
&\quad \left. - (1 - \gamma_\mu) U_\mu(x) G(x + a\hat{\mu}, 0) \sigma_{\nu\lambda} \gamma_5 G^\dagger(x, 0) \gamma_5 \right\rangle \tag{52} \\
&+ \frac{a^5}{4} c_{CVC} \sum_x e^{iq(x-a\hat{\nu}/2)} \hat{q}_\sigma \\
&\quad \text{Tr} \left\langle (1 + \gamma_\nu) U_\nu^\dagger(0) \gamma_5 G^\dagger(x, 0) \gamma_5 \sigma_{\mu\sigma} G(x, a\hat{\nu}) \right. \\
&\quad \left. - (1 - \gamma_\nu) U_\nu(0) \gamma_5 G^\dagger(x, a\hat{\nu}) \gamma_5 \sigma_{\mu\sigma} G(x, 0) \right\rangle \\
&- \frac{a^6}{4} c_{CVC}^2 \sum_x e^{iqx} \hat{q}_\lambda \hat{q}_\sigma \\
&\quad \text{Tr} \left\langle \sigma_{\mu\sigma} G(x, 0) \sigma_{\nu\lambda} \gamma_5 G^\dagger(x, 0) \gamma_5 \right\rangle,
\end{aligned}$$

where the improvement term has been integrated by parts. For $\Pi_{\mu\nu}^{(2)}(\hat{q})$ we obtain

$$\Pi_{\mu\nu}^{(2)}(\hat{q}) = \frac{a}{2} \delta_{\mu\nu} \text{Tr} \left\langle (1 + \gamma_\nu) U_\nu^\dagger(0) G(0, a\hat{\nu}) + (1 - \gamma_\nu) U_\nu(0) G^\dagger(0, a\hat{\nu}) \right\rangle. \quad (53)$$

To compute $\Pi_{\mu\nu}^{(1)}(\hat{q})$ and $\Pi_{\mu\nu}^{(2)}(\hat{q})$ we have to do a minimum of five inversions for each gauge field configuration (and each κ value), which makes the calculation computationally quite expensive, in particular on 32^4 lattices.

Appendix B

Perturbative results

Before we describe the lattice calculation in detail, we present here the perturbative Wilson coefficients c_0 , c_4^F and c_4^G . We will work in the quenched approximation, in which contributions from sea quarks are neglected, and which corresponds to $c_4'^F = 0$.

We write

$$\begin{aligned} c_0(\mu^2, Q^2, m) &= c_0^{(0)}(\mu^2, Q^2, m) + \frac{\alpha_s(\mu^2)}{\pi} C_F c_0^{(1)}(\mu^2, Q^2, m) \\ &+ \left(\frac{\alpha_s(\mu^2)}{\pi} \right)^2 \left(C_F^2 c_0^{(2)}(\mu^2, Q^2, m) + C_F C_A c_0^{(2)'}(\mu^2, Q^2, m) \right) + \dots, \end{aligned} \quad (54)$$

with $C_F = 4/3$ and $C_A = 3$ for $SU(3)$. These coefficients can be found in eqs. (27)-(30) of [5] (recall that $Q^2 \equiv -q^2$). In the \overline{MS} scheme the coefficients $c_0^{(0)}$, $c_0^{(1)}$, $c_0^{(2)}$ and $c_0^{(2)'}$ read

$$c_0^{(0)}(\mu^2, Q^2, \bar{m}) = -\frac{9}{4} \left[\frac{20}{9} - \frac{4}{3} \ln \frac{Q^2}{\mu^2} - 8 \frac{\bar{m}^2}{Q^2} + \left(\frac{4\bar{m}^2}{Q^2} \right)^2 \left(\frac{1}{4} + \frac{1}{2} \ln \frac{Q^2}{\bar{m}^2} \right) \right], \quad (55)$$

$$\begin{aligned} c_0^{(1)}(\mu^2, Q^2, \bar{m}) &= -\frac{9}{4} \left[\frac{55}{12} - 4\zeta(3) - \ln \frac{Q^2}{\mu^2} - \frac{4\bar{m}^2}{Q^2} \left(4 - 3 \ln \frac{Q^2}{\mu^2} \right) \right. \\ &+ \left(\frac{4\bar{m}^2}{Q^2} \right)^2 \left(\frac{1}{24} + \zeta(3) + \frac{11}{8} \ln \frac{Q^2}{\bar{m}^2} \right. \\ &\left. \left. + \frac{3}{4} \ln^2 \frac{Q^2}{\bar{m}^2} - \frac{3}{2} \ln \frac{Q^2}{\bar{m}^2} \ln \frac{Q^2}{\mu^2} \right) \right], \end{aligned} \quad (56)$$

$$\begin{aligned}
c_0^{(2)}(\mu^2, Q^2, \bar{m}) = -\frac{9}{4} \left[-\frac{143}{72} - \frac{37}{6}\zeta(3) + 10\zeta(5) + \frac{1}{8} \ln \frac{Q^2}{\mu^2} \right. \\
\left. - \frac{4\bar{m}^2}{Q^2} \left(\frac{1667}{96} - \frac{5}{12}\zeta(3) - \frac{35}{6}\zeta(5) \right. \right. \\
\left. \left. - \frac{51}{8} \ln \frac{Q^2}{\mu^2} + \frac{9}{4} \ln^2 \frac{Q^2}{\mu^2} \right) \right], \quad (57)
\end{aligned}$$

$$\begin{aligned}
c_0^{(2)'}(\mu^2, Q^2, \bar{m}) = -\frac{9}{4} \left[\frac{44215}{2592} - \frac{227}{18}\zeta(3) - \frac{5}{3}\zeta(5) - \frac{41}{8} \ln \frac{Q^2}{\mu^2} \right. \\
\left. + \frac{11}{24} \ln^2 \frac{Q^2}{\mu^2} + \frac{11}{3} \zeta(3) \ln \frac{Q^2}{\mu^2} \right. \\
\left. - \frac{4\bar{m}^2}{Q^2} \left(\frac{1447}{96} + \frac{4}{3}\zeta(3) - \frac{85}{12}\zeta(5) \right. \right. \\
\left. \left. - \frac{185}{24} \ln \frac{Q^2}{\mu^2} + \frac{11}{8} \ln^2 \frac{Q^2}{\mu^2} \right) \right], \quad (58)
\end{aligned}$$

where $\zeta(3) = 1.20206\dots$ and $\zeta(5) = 1.03693\dots$, and \bar{m} refers to the quark mass at the scale μ in the \overline{MS} scheme. In (55),(56) terms of $\mathcal{O}((\bar{m}^2/Q^2)^3)$ modulo logarithms have been neglected, while in (57),(58) terms $\mathcal{O}((\bar{m}^2/Q^2)^2)$ are dropped.

The Wilson coefficients multiplying the quark and gluon condensate are [6,8]

$$\begin{aligned}
c_4^F(\mu, q) &= -12\pi^2 \left(2 + \frac{2}{3} \frac{\alpha_s(\mu^2)}{\pi} + \dots \right), \\
c_4^G(\mu, q) &= -\pi^2 \left(1 - \frac{11}{18} \frac{\alpha_s(\mu^2)}{\pi} + \dots \right). \quad (59)
\end{aligned}$$

Note that both $m\langle\bar{q}q\rangle$ and $(\alpha_s/\pi)\langle G_{\mu\nu}^2\rangle$ are renormalisation group invariants, which means that they do not depend on μ and the renormalisation scheme. The vacuum polarisation $\Pi(Q^2)$ itself is not an observable, but its derivatives are. Therefore the result (7) can only depend on μ and the scheme in terms of an integration constant (independent of Q^2).

We can use renormalisation group improvement to re-sum the logarithms in higher-order terms. This should lead to a significant improvement, since the fact that we are interested in measurements over a large Q^2 range means that these logarithms are large.

If we calculate the Adler function in the chiral limit from eqs (55)-(58) we find the result

$$D(Q^2) = 3 \left\{ 1 + \frac{\alpha_s(\mu^2)}{\pi} + \left(\frac{\alpha_s(\mu^2)}{\pi} \right)^2 \left[\frac{365}{24} - 11\zeta(3) - \frac{11}{4} \ln \frac{Q^2}{\mu^2} \right] \right\}. \quad (60)$$

We should be able to do better than this because the massless Adler function is known to four loops [3]. We can use this perturbative result for the Adler function to improve the result for c_0 in the chiral limit. In quenched $SU(3)$ we have

$$\begin{aligned} R(s) = & 3 \sum_f e_f^2 \left\{ 1 + \left(\frac{\alpha_s(Q^2)}{\pi} \right) + \left(\frac{\alpha_s(Q^2)}{\pi} \right)^2 \left[\frac{365}{24} - 11\zeta(3) \right] \right. \\ & \left. + \left(\frac{\alpha_s(Q^2)}{\pi} \right)^3 \left[\frac{87029}{288} - \frac{1103}{4}\zeta(3) + \frac{275}{6}\zeta(5) - \frac{121}{48}\pi^2 \right] \right\} \\ & + (\sum_f e_f)^2 \left(\frac{\alpha_s(Q^2)}{\pi} \right)^3 \left[\frac{55}{72} - \frac{5}{3}\zeta(3) \right] + \mathcal{O}(\alpha_s^4) \end{aligned} \quad (61)$$

and

$$\begin{aligned} D(Q^2) = & 3 \sum_f e_f^2 \left\{ 1 + \left(\frac{\alpha_s(Q^2)}{\pi} \right) + \left(\frac{\alpha_s(Q^2)}{\pi} \right)^2 \left[\frac{365}{24} - 11\zeta(3) \right] \right. \\ & \left. + \left(\frac{\alpha_s(Q^2)}{\pi} \right)^3 \left[\frac{87029}{288} - \frac{1103}{4}\zeta(3) + \frac{275}{6}\zeta(5) \right] \right\} \\ & + (\sum_f e_f)^2 \left(\frac{\alpha_s(Q^2)}{\pi} \right)^3 \left[\frac{55}{72} - \frac{5}{3}\zeta(3) \right] + \mathcal{O}(\alpha_s^4). \end{aligned} \quad (62)$$

Note that although the first terms of R and D coincide, the α_s^3 term is different. The extra " π^2 " term in R arises from analytic continuation, $\ln^3(Q^2/\mu^2) \rightarrow [\ln(s/\mu^2) \pm i\pi]^3$, see [3]. The first part of (62), proportional to $\sum_f e_f^2$, is the derivative of the C_Π term in (6), while the second term, proportional to $(\sum_f e_f)^2$, comes from the derivative of the A_Π term.

From (62) we have a differential equation for c_0 :

$$Q^2 \frac{\partial}{\partial Q^2} c_0(\mu^2, Q^2, m=0) = 3 \left\{ 1 + \left(\frac{\alpha_s(Q^2)}{\pi} \right) + \left(\frac{\alpha_s(Q^2)}{\pi} \right)^2 \left[\frac{365}{24} - 11\zeta(3) \right] + \left(\frac{\alpha_s(Q^2)}{\pi} \right)^3 \left[\frac{87029}{288} - \frac{1103}{4} \zeta(3) + \frac{275}{6} \zeta(5) \right] + \mathcal{O}(\alpha_s^4) \right\}. \quad (63)$$

We can solve this by using the known β -function [28]

$$Q^2 \frac{\partial}{\partial Q^2} \left(\frac{\alpha_s(Q^2)}{\pi} \right) = - \sum_i \beta_i \left(\frac{\alpha_s(Q^2)}{\pi} \right)^{i+2} \quad (64)$$

with

$$\beta_0 = \frac{11}{4}, \quad \beta_1 = \frac{51}{8}, \quad \beta_2 = \frac{2857}{128}, \quad \beta_3 = \frac{149753}{1536} + \frac{891}{64} \zeta(3) \quad (65)$$

in the case of quenched $SU(3)$.

The solution is

$$c_0(\mu^2, Q^2, 0) = 3 \ln Q^2 - \frac{12}{11} \ln(\alpha_s(Q^2)) + \left[-\frac{3403}{242} + 12\zeta(3) \right] \frac{\alpha_s(Q^2)}{\pi} \quad (66) \\ + \left[-\frac{2301587}{15972} + \frac{273}{2} \zeta(3) - 25\zeta(5) \right] \left(\frac{\alpha_s(Q^2)}{\pi} \right)^2 + \mathcal{O}(\alpha_s^3) + \text{const.}$$

The constant of integration can be fixed by comparing with (54)-(58), giving the final renormalisation group improved result²

$$c_0(\mu^2, Q^2, 0) = 3 \ln \frac{Q^2}{\mu^2} - \frac{12}{11} \ln \left[\frac{\alpha_s(Q^2)}{\alpha_s(\mu^2)} \right] + \left[-\frac{3403}{242} + 12\zeta(3) \right] \frac{\alpha_s(Q^2)}{\pi} \\ + \left[-\frac{2301587}{15972} + \frac{273}{2} \zeta(3) - 25\zeta(5) \right] \left(\frac{\alpha_s(Q^2)}{\pi} \right)^2 \quad (67) \\ - 5 + \frac{151}{484} \frac{\alpha_s(\mu^2)}{\pi} + \left[-\frac{566749}{383328} + \frac{5}{3} \zeta(3) \right] \left(\frac{\alpha_s(\mu^2)}{\pi} \right)^2 \\ + O(\alpha_s^3(Q^2), \alpha_s^3(\mu^2))$$

where μ is the \overline{MS} scale.

² Note the interesting result that due to a cancellation there is no $\zeta(3)$ term in the coefficient of $\alpha_s(\mu^2)$ and no $\zeta(5)$ in the coefficient of $\alpha_s(\mu^2)^2$. This surprised us.

One can check that the differences between (67) and (54) are indeed $O(\alpha_s^3)$ by making the substitution

$$\begin{aligned} \frac{\alpha_s(Q^2)}{\pi} \rightarrow \frac{\alpha_s(\mu^2)}{\pi} - \beta_0 \left(\frac{\alpha_s(\mu^2)}{\pi} \right)^2 \ln \frac{Q^2}{\mu^2} - \beta_1 \left(\frac{\alpha_s(\mu^2)}{\pi} \right)^3 \ln \frac{Q^2}{\mu^2} \\ + \beta_0^2 \left(\frac{\alpha_s(\mu^2)}{\pi} \right)^3 \ln^2 \frac{Q^2}{\mu^2} + \mathcal{O}(\alpha_s^4) \end{aligned} \quad (68)$$

in (67).

Renormalisation group improvement of the mass terms in (55)-(58) is simpler because there is no constant of integration involved. The result is

$$\begin{aligned} c_0(\mu^2, Q^2, \bar{m}) = c_0(\mu^2, Q^2, 0) + \frac{m_{\overline{MS}}^2(Q^2)}{Q^2} \left\{ 18 + 48 \frac{\alpha_s(Q^2)}{\pi} \right. \\ \left. + \left[\frac{19691}{24} + \frac{124}{3} \zeta(3) - \frac{1045}{3} \zeta(5) \right] \left(\frac{\alpha_s(Q^2)}{\pi} \right)^2 \right\} \\ + \left(\frac{m_{\overline{MS}}^2(Q^2)}{Q^2} \right)^2 \left\{ -9 - 18 \ln \frac{Q^2}{m_{\overline{MS}}^2(Q^2)} \right. \\ \left. - \left[2 + 48 \zeta(3) + 66 \ln \frac{Q^2}{m_{\overline{MS}}^2(Q^2)} + 36 \ln^2 \frac{Q^2}{m_{\overline{MS}}^2(Q^2)} \right] \frac{\alpha_s(Q^2)}{\pi} \right\}. \end{aligned} \quad (69)$$

What have we gained by using the renormalisation group? Most importantly, the Q^2 derivative of (67) is correct to four loops, one order better than (54). The uncertainties in (67) are $\mathcal{O}(\alpha_s^3(Q^2), \alpha_s^3(\mu^2))$ while in the original formula (54) terms of order $\mathcal{O}(\alpha_s^3(\mu^2) \ln^3(Q^2/\mu^2))$ have been neglected. So, if we are interested in describing a large range of Q^2 , eq.(67) ought to be the better formula. In addition, (67) exhibits correct physics, because it is the sum of a piece depending only on Q^2 and a piece depending only on μ^2 , which is only approximately the case for (54).

Appendix C

In the following Tables we give the results for $C_{\Pi}(\hat{q}, am)$ at the various β and κ values. We label the lattice momenta by the vector n , $\hat{q}_\mu = (2/a) \sin(\pi n_\mu/L)$. The momenta were chosen close to the diagonal of the Brillouin zone to avoid large $\mathcal{O}(a^2)$ effects.

n	$\kappa = 0.1333$	$\kappa = 0.1339$	$\kappa = 0.1342$	$\kappa = 0.1345$
(1,0,0,0)	-38.15(11)	-38.60(15)	-38.84(14)	-39.03(16)
(1,1,0,0)	-36.59(10)	-36.89(13)	-37.05(12)	-37.17(13)
(1,1,1,0)	-35.52(09)	-35.75(12)	-35.89(11)	-35.99(12)
(1,1,1,1)	-34.72(09)	-34.91(12)	-35.04(11)	-35.12(12)
(2,1,1,1)	-32.89(08)	-33.06(10)	-33.15(09)	-33.24(10)
(2,2,1,1)	-31.82(07)	-31.98(10)	-32.07(09)	-32.15(10)
(2,2,2,1)	-31.07(07)	-31.22(09)	-31.30(08)	-31.40(09)
(2,2,2,2)	-30.47(07)	-30.62(09)	-30.71(08)	-30.81(09)
(3,2,2,2)	-29.61(06)	-29.76(09)	-29.85(08)	-29.95(09)
(3,3,2,2)	-28.98(06)	-29.13(08)	-29.22(08)	-29.32(08)
(3,3,3,2)	-28.47(06)	-28.63(08)	-28.72(07)	-28.82(08)
(3,3,3,3)	-28.05(06)	-28.20(08)	-28.29(07)	-28.39(08)
(4,3,3,3)	-27.54(05)	-27.70(08)	-27.79(07)	-27.89(08)
(4,4,3,3)	-27.12(05)	-27.28(07)	-27.37(07)	-27.47(08)
(4,4,4,3)	-26.76(05)	-26.91(07)	-27.00(07)	-27.11(07)
(4,4,4,4)	-26.42(05)	-26.58(07)	-26.67(07)	-26.78(07)
(5,4,4,4)	-26.11(05)	-26.26(07)	-26.36(06)	-26.46(07)
(5,5,4,4)	-25.82(05)	-25.97(07)	-26.07(06)	-26.17(07)
(5,5,5,4)	-25.55(05)	-25.70(07)	-25.80(06)	-25.90(07)
(5,5,5,5)	-25.29(05)	-25.44(07)	-25.54(06)	-25.64(07)
(6,5,5,5)	-25.09(05)	-25.25(06)	-25.34(06)	-25.45(07)
(6,6,5,5)	-24.90(04)	-25.05(06)	-25.15(06)	-25.25(06)
(6,6,6,5)	-24.71(04)	-24.86(06)	-24.96(06)	-25.06(06)
(6,6,6,6)	-24.52(04)	-24.67(06)	-24.77(06)	-24.87(06)
(7,6,6,6)	-24.42(04)	-24.57(06)	-24.67(05)	-24.77(06)
(7,7,6,6)	-24.31(04)	-24.46(06)	-24.56(05)	-24.66(06)
(7,7,7,6)	-24.19(04)	-24.34(06)	-24.44(05)	-24.54(06)
(7,7,7,7)	-24.07(04)	-24.22(06)	-24.32(05)	-24.42(06)

Table 5
The vacuum polarisation $C_{\Pi}(\hat{q}^2, am)$ on the 16^4 lattice at $\beta = 6.0$.

n	$\kappa = 0.1345$
(1,0,0,0)	-41.64(22)
(1,1,0,0)	-40.67(19)
(1,1,1,0)	-39.85(17)
(1,1,1,1)	-39.16(16)
(2,1,1,1)	-37.58(14)
(2,2,1,1)	-36.51(13)
(2,2,2,1)	-35.72(13)
(2,2,2,2)	-35.09(12)
(3,2,2,2)	-34.20(12)
(3,3,2,2)	-33.52(11)
(3,3,3,2)	-32.99(11)
(3,3,3,3)	-32.54(11)
(4,3,3,3)	-31.97(11)
(4,4,3,3)	-31.50(10)
(4,4,4,3)	-31.11(10)
(4,4,4,4)	-30.77(10)
(5,4,4,4)	-30.36(10)
(5,5,4,4)	-30.01(10)
(5,5,5,4)	-29.70(10)
(5,5,5,5)	-29.43(9)
(6,5,5,5)	-29.11(9)
(6,6,5,5)	-28.84(9)
(6,6,6,5)	-28.59(9)
(6,6,6,6)	-28.36(9)
(7,6,6,6)	-28.11(9)
(7,7,6,6)	-27.88(9)
(7,7,7,6)	-27.68(9)
(7,7,7,7)	-27.48(9)

Table 6
The vacuum polarisation $C_{\Pi}(\hat{q}^2, am)$ on the 32^4 lattice at $\beta = 6.0$.

n	$\kappa = 0.1344$	$\kappa = 0.1349$	$\kappa = 0.1352$
(1,0,0,0)	-40.24(14)	-40.87(17)	-41.16(16)
(1,1,0,0)	-38.78(12)	-39.17(14)	-39.35(12)
(1,1,1,0)	-37.74(11)	-38.03(13)	-38.17(11)
(1,1,1,1)	-36.96(10)	-37.19(12)	-37.30(11)
(2,1,1,1)	-35.23(09)	-35.40(10)	-35.47(09)
(2,2,1,1)	-34.16(08)	-34.31(09)	-34.38(08)
(2,2,2,1)	-33.39(07)	-33.54(08)	-33.60(07)
(2,2,2,2)	-32.79(07)	-32.94(08)	-33.00(07)
(3,2,2,2)	-31.93(06)	-32.08(07)	-32.13(07)
(3,3,2,2)	-31.29(06)	-31.44(07)	-31.49(06)
(3,3,3,2)	-30.78(06)	-30.94(07)	-30.99(06)
(3,3,3,3)	-30.35(06)	-30.52(06)	-30.57(06)
(4,3,3,3)	-29.81(06)	-29.98(06)	-30.03(06)
(4,4,3,3)	-29.37(06)	-29.54(06)	-29.59(06)
(4,4,4,3)	-28.99(05)	-29.17(06)	-29.22(06)
(4,4,4,4)	-28.67(05)	-28.84(06)	-28.90(05)
(5,4,4,4)	-28.29(05)	-28.46(06)	-28.52(05)
(5,5,4,4)	-27.96(05)	-28.14(05)	-28.20(05)
(5,5,5,4)	-27.67(05)	-27.85(05)	-27.91(05)
(5,5,5,5)	-27.41(05)	-27.58(05)	-27.64(05)
(6,5,5,5)	-27.12(05)	-27.30(05)	-27.37(05)
(6,6,5,5)	-26.87(05)	-27.05(05)	-27.11(05)
(6,6,6,5)	-26.64(05)	-26.82(05)	-26.89(05)
(6,6,6,6)	-26.42(05)	-26.60(05)	-26.66(05)
(7,6,6,6)	-26.21(05)	-26.39(05)	-26.45(05)
(7,7,6,6)	-26.01(05)	-26.19(05)	-26.26(05)
(7,7,7,6)	-25.82(04)	-26.00(05)	-26.07(04)
(7,7,7,7)	-25.64(04)	-25.82(05)	-25.89(04)

Table 7
The vacuum polarisation $C_{\Pi}(\hat{q}^2, am)$ on the 24^4 lattice at $\beta = 6.2$.

n	$\kappa = 0.1346$	$\kappa = 0.1350$	$\kappa = 0.1352$
(1,0,0,0)	-41.88(16)	-42.52(22)	-42.84(18)
(1,1,0,0)	-40.38(15)	-40.77(19)	-40.97(15)
(1,1,1,0)	-39.33(14)	-39.61(17)	-39.75(14)
(1,1,1,1)	-38.53(13)	-38.74(17)	-38.86(14)
(2,1,1,1)	-36.82(11)	-36.96(13)	-37.02(11)
(2,2,1,1)	-35.73(10)	-35.84(11)	-35.89(10)
(2,2,2,1)	-34.93(09)	-35.04(10)	-35.09(09)
(2,2,2,2)	-34.31(08)	-34.42(10)	-34.46(08)
(3,2,2,2)	-33.44(08)	-33.55(08)	-33.58(08)
(3,3,2,2)	-32.79(07)	-32.89(08)	-32.93(07)
(3,3,3,2)	-32.27(07)	-32.37(07)	-32.41(07)
(3,3,3,3)	-31.83(06)	-31.94(07)	-31.98(06)
(4,3,3,3)	-31.28(06)	-31.39(06)	-31.42(06)
(4,4,3,3)	-30.83(06)	-30.94(06)	-30.98(06)
(4,4,4,3)	-30.45(05)	-30.56(06)	-30.60(05)
(4,4,4,4)	-30.12(05)	-30.23(06)	-30.28(05)
(5,4,4,4)	-29.73(05)	-29.84(05)	-29.88(05)
(5,5,4,4)	-29.39(05)	-29.51(05)	-29.55(05)
(5,5,5,4)	-29.09(05)	-29.21(05)	-29.25(05)
(5,5,5,5)	-28.83(04)	-28.95(05)	-28.99(05)
(6,5,5,5)	-28.53(04)	-28.65(05)	-28.69(04)
(6,6,5,5)	-28.26(04)	-28.39(05)	-28.43(04)
(6,6,6,5)	-28.02(04)	-28.15(04)	-28.19(04)
(6,6,6,6)	-27.80(04)	-27.93(04)	-27.97(04)
(7,6,6,6)	-27.56(04)	-27.70(04)	-27.74(04)
(7,7,6,6)	-27.35(04)	-27.48(04)	-27.52(04)
(7,7,7,6)	-27.15(04)	-27.28(04)	-27.32(04)
(7,7,7,7)	-26.96(04)	-27.10(04)	-27.14(04)

Table 8
The vacuum polarisation $C_{\Pi}(\hat{q}^2, am)$ on the 32^4 lattice at $\beta = 6.4$.

References

- [1] F.J. Reinders, H. Rubinstein and S. Yazaki, Phys. Rep. 127 (1985) 1; S. Narison, “QCD Spectral Sum Rules”, World Scientific, 1989.
- [2] S.L. Adler, Phys. Rev. D10 (1974) 3714.
- [3] S.G. Gorishny, A.L. Kataev and S.A. Larin, Phys. Lett. B 259 (1991) 144; L.R. Surguladze and M.A. Samuel, Phys. Rev. Lett. 66 (1991) 560, *erratum ibid* 2416.
- [4] K.G. Chetyrkin, Phys. Lett. B391 (1997) 402 (hep-ph/9608480).
- [5] K.G. Chetyrkin, J.H. Kühn and M. Steinhauser, Nucl. Phys. B482 (1996) 213.
- [6] M.A. Shifman, A.I. Vainshtein and V.I. Zakharov, Nucl. Phys. B147 (1979) 385.
- [7] M.A. Shifman, A.I. Vainshtein and V.I. Zakharov, Nucl. Phys. B147 (1979) 448.
- [8] S.C. Generalis, J. Phys. G15 (1989) L225; K.G. Chetyrkin, S.G. Gorishny and V.P. Spiridonov, Phys. Lett. 160B (1985) 149; V.P. Spiridonov and K.G. Chetyrkin, Yad. Fiz. 47 (1988) 818 [Sov. J. Nucl. Phys. 47 (1988) 522].
- [9] S. Eidelman, F. Jegerlehner, A.L. Kataev and O. Veretin, Phys. Lett. B454 (1999) 369 (hep-ph/9812521).
- [10] M. Göckeler, R. Horsley, W. Kürzinger, V. Linke, D. Pleiter, P.E.L. Rakow and G. Schierholz, Nucl. Phys. (Proc. Suppl.) 94 (2001) 571 (hep-lat/0012010); M. Göckeler, R. Horsley, W. Kürzinger, V. Linke, D. Pleiter, P.E.L. Rakow and G. Schierholz, (hep-lat/0310027).
- [11] M. Göckeler, R. Horsley, H. Perlt, P. Rakow, G. Schierholz, A. Schiller and P. Stephenson, Phys. Rev. D57 (1998) 5562. (hep-lat/9707021).
- [12] M. Göckeler, P.E.L. Rakow, R. Horsley, D. Petters, D. Pleiter and G. Schierholz, in *Lattice fermions and structure of the vacuum*, p. 201, eds. V. Mitrjushkin and G. Schierholz (Kluwer, Dordrecht, 2000); M. Göckeler, R. Horsley, D. Petters, D. Pleiter, P.E.L. Rakow, G. Schierholz and P. Stephenson, Nucl. Phys. (Proc. Suppl.) 83 (2000) 203 (hep-lat/9909160).
- [13] M. Göckeler et al., in preparation.
- [14] W. Kürzinger, Ph.D. Thesis (in German), Freie Universität Berlin (2001); <http://www.diss.fu-berlin.de/2001/220/>
- [15] “Quantum Fields on a Lattice”, I. Montvay and G. Münster, CUP 1994.
- [16] S. Capitani, M. Göckeler, R. Horsley, H. Perlt, P.E.L. Rakow, G. Schierholz and A. Schiller, Nucl. Phys. B593 (2001) 183.
- [17] M. Lüscher, S. Sint, R. Sommer, P. Weisz and U. Wolff, Nucl. Phys. B491 (1997) 323.

- [18] S. Booth, M. Göckeler, R. Horsley, A.C. Irving, B. Joo, S. Pickles, D. Pleiter, P.E.L. Rakow, G. Schierholz, Z. Sroczynski and H. Stüben, *Phys. Lett.* B519 (2001) 229.
- [19] S. Capitani, M. Lüscher, R. Sommer and H. Wittig, *Nucl. Phys.* B544 (1999) 669; P. Boucaud, G. Burgio, F. Di Renzo, J.P. Leroy, J. Micheli, C. Parrinello, O. Pène, C. Pittori, J. Rodriguez-Quintero, C. Roiesnel and K. Sharkey, *JHEP* 0004 (2000) 006.
- [20] M. Guagnelli, R. Sommer and H. Wittig, *Nucl. Phys.* B535 (1998) 389.
- [21] O. Dumbrajs, R. Koch, H. Pilkuhn, G.C. Oades, H. Behrens, J.J. De Swart and P. Kroll, *Nucl. Phys.* B216 (1983) 277.
- [22] Review of Particle Physics, K. Hagiwara et al., *PR D66* (2002) 010001.
- [23] R.A. Bertlmann, G. Launer and E. de Rafael, *Nucl. Phys.* B250 (1985) 61.
- [24] T. Blum, *Phys. Rev. Lett.* 91 (2003) 052001; T. Blum, [hep-lat/0310064](#).
- [25] A. Nyffeler, [hep-ph/0305135](#).
- [26] S. Eidelman and F. Jegerlehner, *Z. Phys. C* **67** (1995) 585
- [27] F. Jegerlehner, *J. Phys. G* 29 (2003) 101; K. Hagiwara, A.D. Martin, D. Nomura and T. Teubner, *Phys. Lett. B* 557 (2003) 69; K. Hagiwara, A.D. Martin, D. Nomura and T. Teubner, [hep-ph/0312250](#); M. Davier, S. Eidelman, A. Hocker and Z. Zhang, *Eur. Phys. J. C* 27 (2003) 497.
- [28] T. van Ritbergen, J.A.M. Vermaseren and S.A. Larin, *Phys. Lett.* B400 (1997) 379; J.A.M. Vermaseren and S.A. Larin and T. van Ritbergen, *Phys. Lett.* B405 (1997) 327.